中国科学院高能物理研究所
Institute of High Energy Physics
Chinese Academy of Sciences

A Novel Hybrid Cherenkov–Scintillation Compton Camera for MeV Gamma-Ray Imaging

Qiuping SHEN, Lei Cao, Okawa Hideki, Xianchao Huang, Tao Liu,
Min Ouyang, Wenxi Peng, Xilei Sun, Mingzheng Yang, Jingbo Ye

IHEP, CAS

Experimental Physics Division Seminar

2026-05-26

Research Background

- Gamma-ray imaging has broad applications in astrophysics, nuclear physics, medical imaging, radiation monitoring, and nuclear security.

1. Mechanical collimation

Simple and widely used, but suffers from very low detection efficiency; spatial resolution and sensitivity cannot be optimized simultaneously.

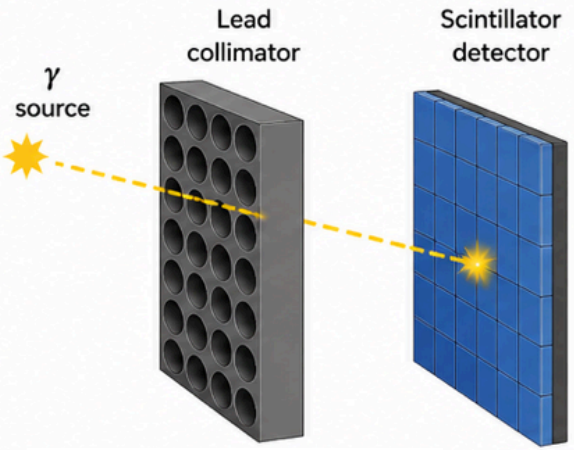

Schematic illustrations

- ✓ Simple structure, mature technology
- ✗ Very low detection efficiency (most photons are blocked)
- ✗ Spatial resolution and sensitivity cannot be optimized simultaneously

2. Traditional Compton camera without electron direction

Reconstructs a Compton cone from energy and position measurements, but single-event source direction remains ambiguous and requires many events for image formation.

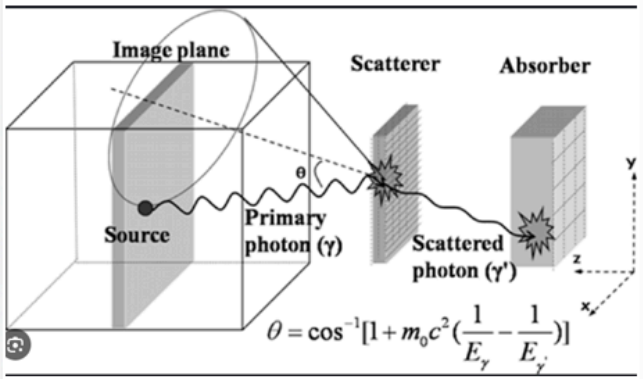

- ✓ Higher efficiency than mechanical collimation
- ✗ Cone ambiguity: source lies somewhere on the cone
- ✗ Single-event direction is ambiguous, requires many events for imaging

3. Electron-tracking Compton camera

Can reduce cone ambiguity by measuring recoil-electron direction, but usually requires complex silicon tracking layers or bulky TPC systems, increasing detector size, cost, and readout complexity.

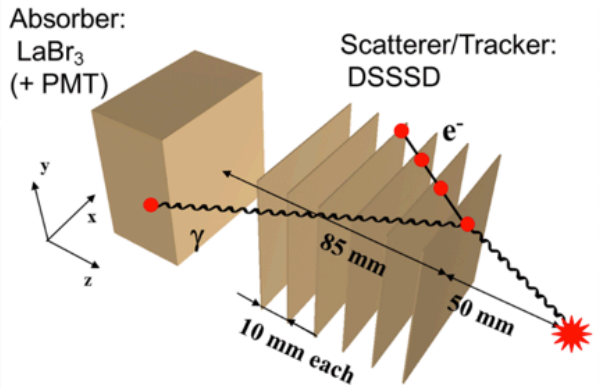

epjconf_inpc2013_11036.pdf

- ✓ Reduces cone ambiguity with electron direction information
- ✗ Requires complex silicon tracking layers or bulky TPC systems
- ✗ Larger size, higher cost, more complex readout

Hybrid Compton Camera Geometry

1. Detector Concept (Exterior View)

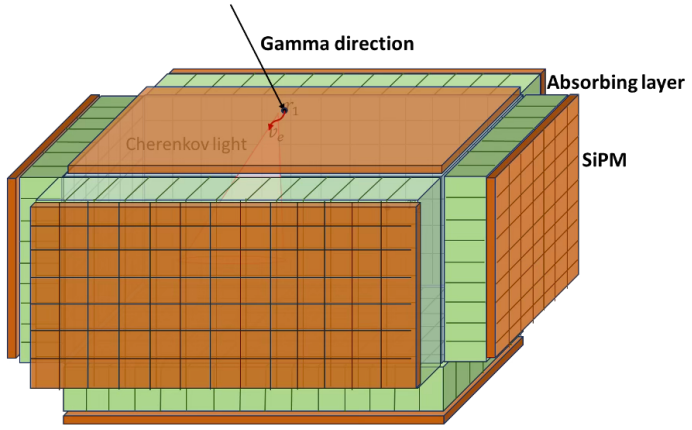

2. Detector Concept (Interior View)

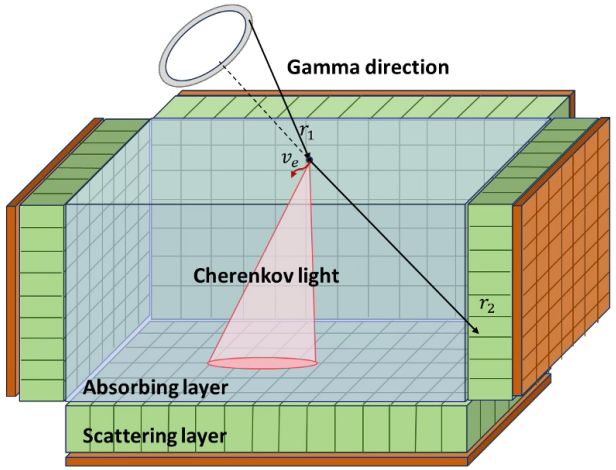

3. Side View (Cross Section)

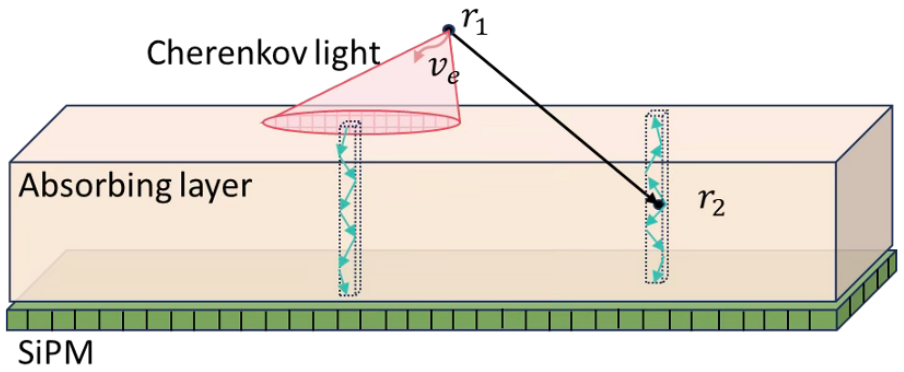

4. Geometry Summary

- Central CsI cube (scattering layer): 5 cm × 5 cm × 5 cm
- BGO bar absorber layers on five faces: +X, −X, +Y, −Y, +Z (−Z face is open)
- Six SiPM planes outside the absorber system on all faces (+X, −X, +Y, −Y, +Z, −Z)
- BGO bars are wrapped with reflective silicone (Teflon-like)
- SiPM planes are located outside the absorber system on all six faces

5. Key Dimensions

CsI cube (scattering layer)	5.0 × 5.0 × 5.0 cm³
BGO bar (core)	0.18 × 0.18 × 0.50 cm³
Silicone wrapper thickness	0.01 cm
Pitch (wrapped)	0.20 cm
Bars per side	25
Bars per face	25 × 25 = 625
Absorber faces	5 (±X, ±Y, +Z)
Open face	−Z

6. Optical / Physical Processes

1. Gamma ray (γ) enters from the open −Z face.
2. First interaction occurs in CsI at γ_1 via Compton scattering.
3. Recoil electron (v_e) is emitted and produces Cherenkov light in CsI.
4. Scattered gamma (γ_2) travels a distance r_2 and is absorbed in the BGO absorber layer.
5. Cherenkov photons propagate and are detected by the surrounding SiPM planes on all six faces.

7. Materials & Optical Properties

- CsI (Scattering Layer)
  Density: 4.51 g/cm³
  Refractive index: ~ 1.79
  Emission: Cherenkov
- BGO (Absorber Layer)
  Density: 7.13 g/cm³
  Refractive index: ~ 2.15
  Scintillation: ~ 480 nm
- Silicone Wrapper (Reflective)
  (Teflon-like) Reflectivity: ~ 0.95
- Si (SiPM Planes)
  PDE: high (wavelength dependent)

Summary: A hybrid Cherenkov–scintillation Compton camera in which a 5 cm CsI scattering cube is surrounded by BGO bar absorber layers on five faces. Cherenkov light from the recoil electron is detected by SiPM planes on all six faces, enabling electron–direction measurement without tracking detectors.

Optical Photon Signatures in the Hybrid Detector

- CsI(Tl) scintillation from recoil-electron energy deposition:
  - Nearly isotropic emission; Slow decay time (~1 μs); Large photon yield, Broad time distribution
  - Provides energy and position P_1 information for the first interaction.
- BGO scintillation from scattered-γ energy deposition:
  - Nearly isotropic emission; Fast decay time (~300 ns); Large photon yield, Narrower time profile than CsI(Tl)
  - Provides energy and position P_2 information for the second interaction.
- Cherenkov photons from recoil electrons in CsI(Tl):
  - Prompt ps-scale emission; very early arrival times; Directional emission with the recoil-electron direction
  - Much lower photon yield, but high directional information content

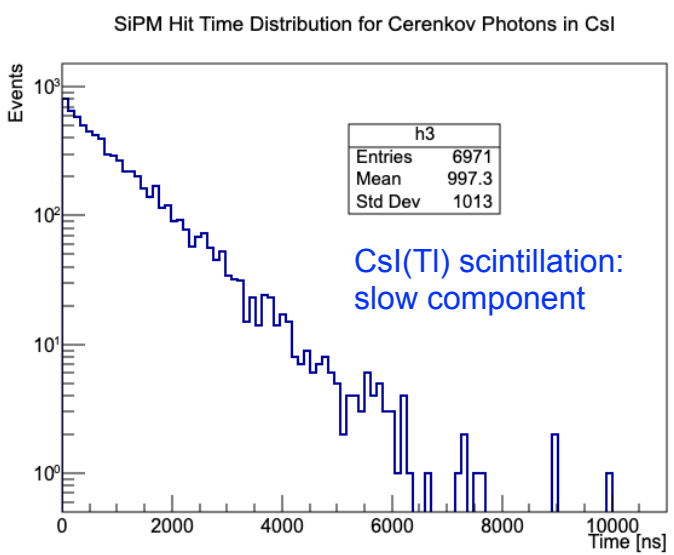

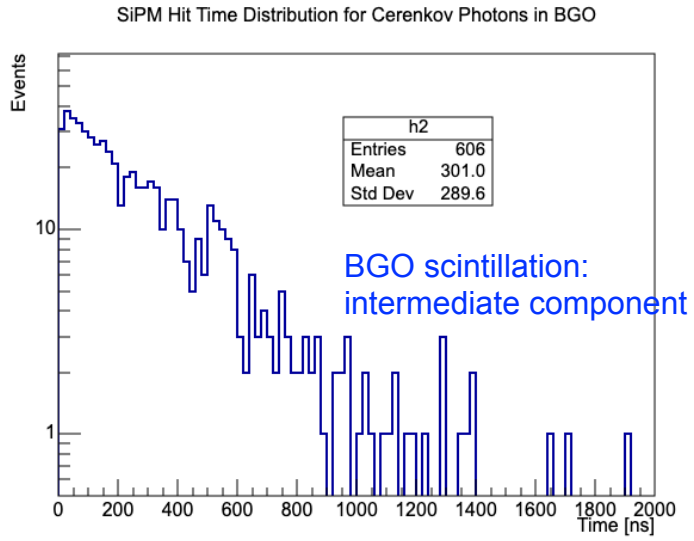

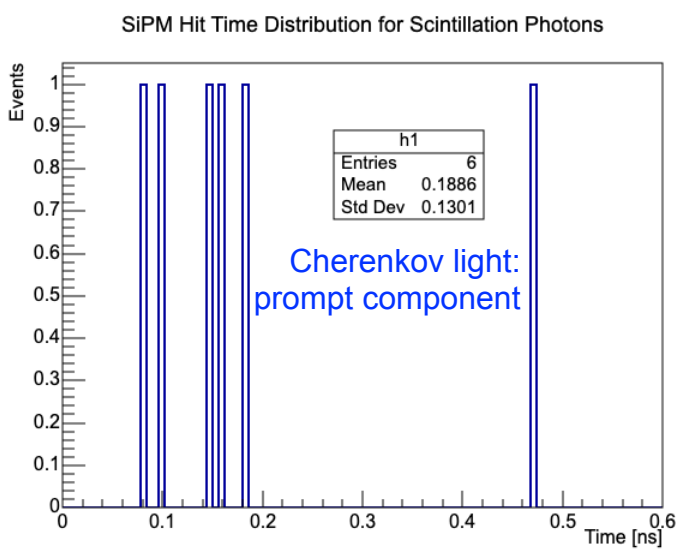

Geant4 Simulation

- A Geant4-based simulation framework was developed for the proposed Compton camera geometry.
- The final target focuses on the 1–10 MeV gamma-ray energy range.

- As an initial benchmark, preliminary studies used 1 MeV gamma rays from a fixed point source.
  - Source position: (0, 0, −28 mm), 3 mm upstream of the incident face at z = −25 mm.
  - Currently focused on Compton process:
    - Selected events require the first interaction in the CsI scatterer and full energy deposition in BGO absorber bars.
  - To investigate the pair production and multi-scattering process (may work using the advanced deep learning reconstruction algorithms).

- The simulation and data-processing workflow is summarized below.

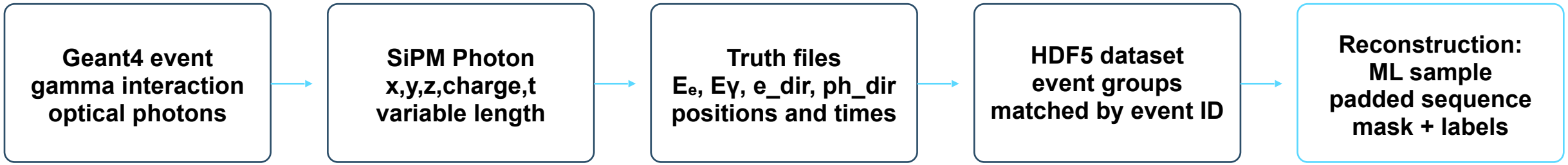

Detector Energy Calibration

- Using electrons with varied energies (at the center)
- Count the total photons in all six faces (ignoring PDE)

- Energy in CsI(Tl) (55000/MeV) calibrated with electrons:

Energy/MeV	N. photons	Std.
0.2	8533	98
0.4	17050	549
0.6	25575	1053
0.8	34027	1880
1	42539	2154

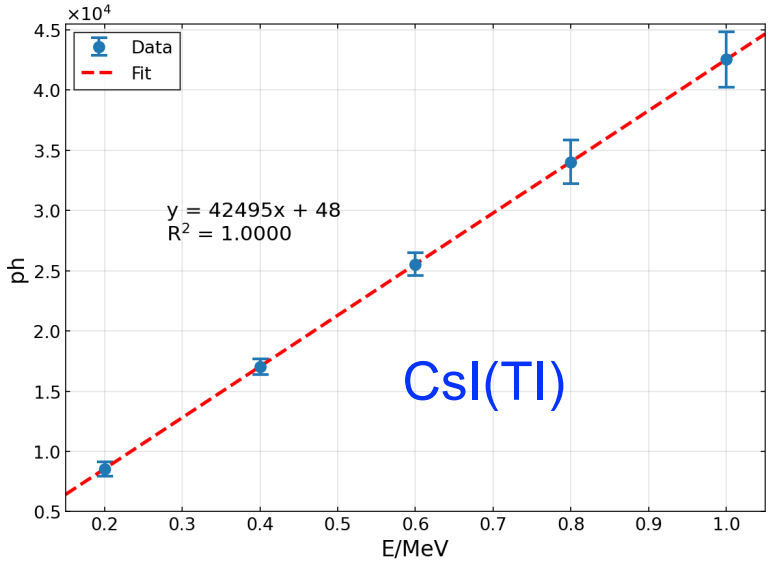

- Energy in BGO (8000/MeV) calibrated with electrons:

Energy/MeV	N. photons	Std.
0.2	916	29
0.4	1257	491
0.6	2804	627
0.8	3816	1423
1	4852	2386

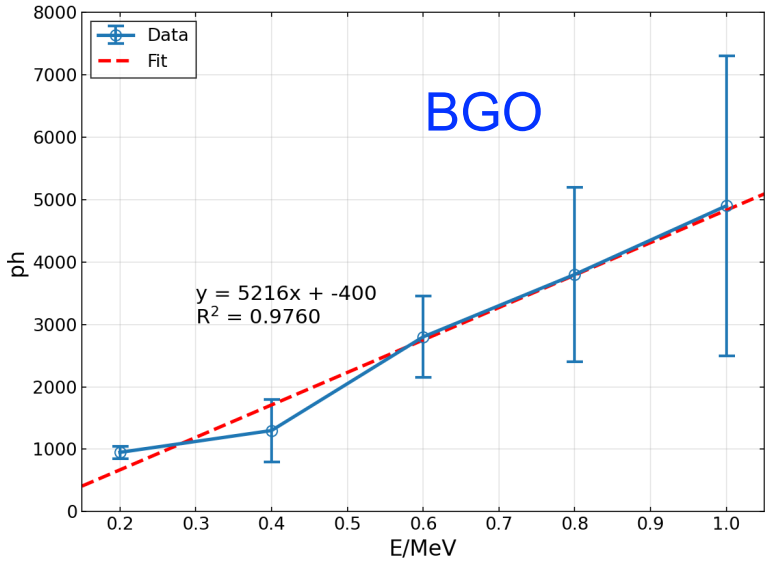

Common Reconstruction Algorithm: Likelihood

1 Select "good" topology

- First interaction in CsI(Tl) = Compton
- Second interaction in BGO = photoelectric

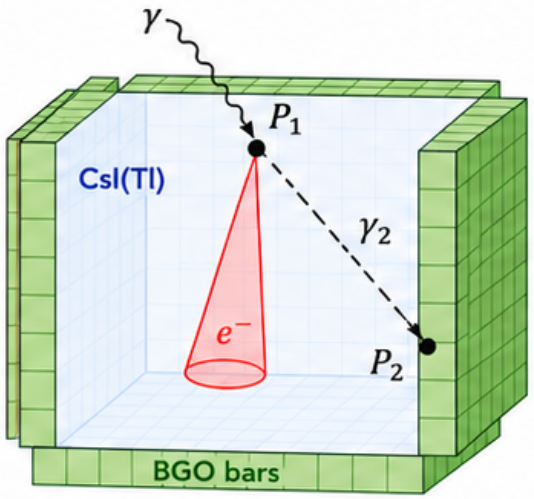

Calibrate E_1 and E_2 from optical photon yields

2 Reconstruct P_1 in CsI(Tl) with maximum likelihood

- Get recoil-electron direction from early Cherenkov photons

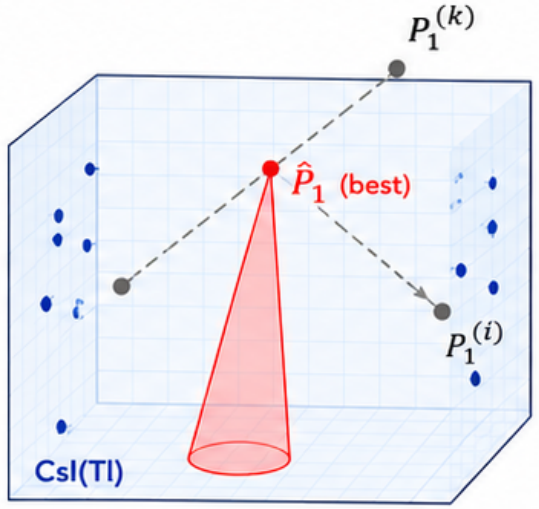

Likelihood $L(P_1, \hat{d}_e)$ from Cherenkov hit pattern

3 Select brightest BGO spot (no likelihood)

- Select P_2 as the brightest BGO spot
- Get scattered-photon direction from $P_1 \rightarrow P_2$

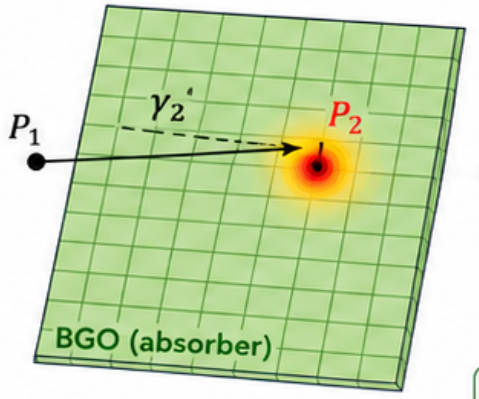

Select P_2 as brightest BGO (no likelihood)

4 Infer incident gamma direction

- Combine Compton kinematics + electron direction
- Reconstruct incident gamma direction $\hat{n}_\gamma$

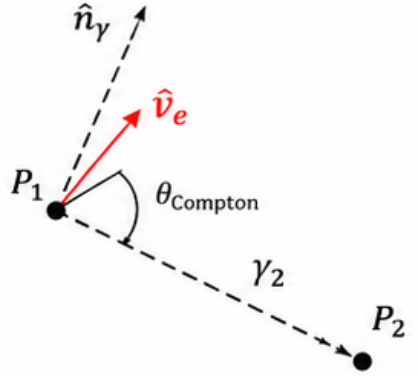

Compton kinematics

$$\cos\theta_{\text{Compton}} = 1 - m_e c^2 \left(\frac{1}{E_2} - \frac{1}{E_1 + E_2}\right)$$

Output

$\hat{n}_\gamma$ (incident gamma direction)

Dominant Bottlenecks

P_2 mis-identification strongly biases BGO energy and scattered-photon direction.

P_1 has a noticeable depth bias, especially in z direction.

Electron-direction reconstruction is still much weaker than photon-direction reconstruction.

Error Propagation Cascade (Drives Final Direction Error)

Position Error $(\delta P_1, \delta P_2)$

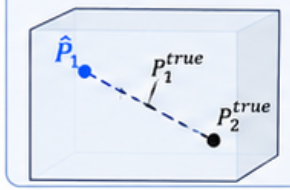

Recoil Electron Direction Error $(\delta \hat{v}_e)$

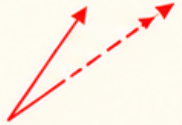

Scattering Photon Direction Error $(\delta \hat{\gamma}_2)$

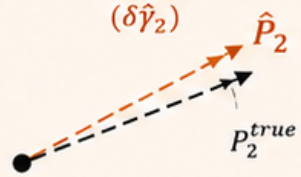

Incident Gamma Direction Error $(\delta \hat{n}_\gamma)$

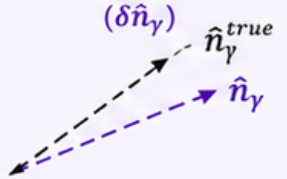

Position error → recoil electron / scattering photon opening-angle error → gamma-direction error
(Used the transformer algorithm to reconstruct the directions.)

Likelihood-Based Reconstruction Baseline

- A likelihood-based reconstruction was tested as a conventional baseline method.
- The reconstructed angular errors are relatively large:
  - Recoil electron: mean ≈ 47.9°; Scattered photon: mean ≈ 21.6°; Incident gamma: mean ≈ 40.8°

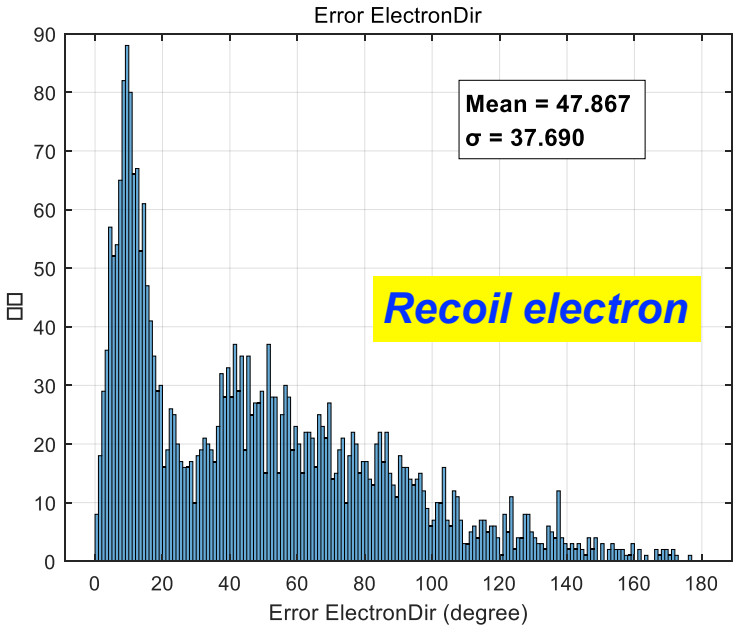

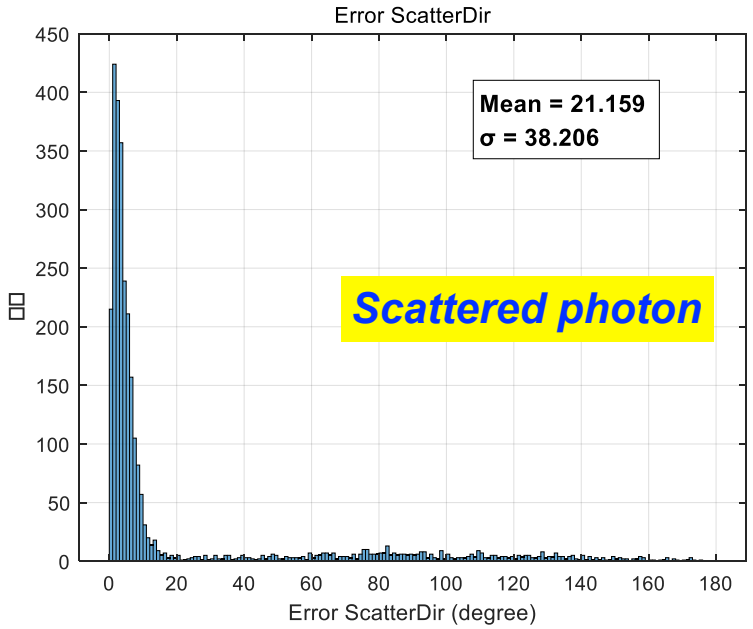

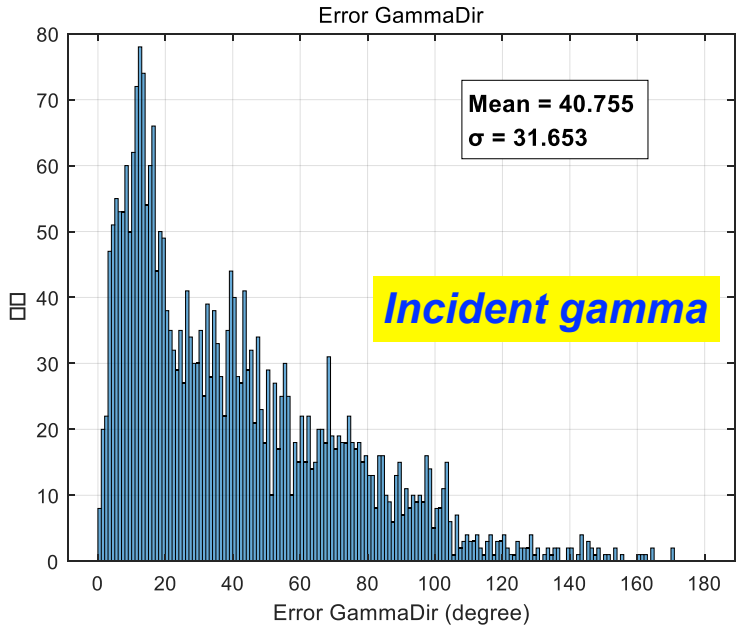

- The poor incident-gamma performance suggests that the available detector information is difficult to exploit with a simple likelihood model.
- This motivates Transformer-based reconstruction using the full SiPM photon-hit topology.

Simulation Strategy for Training and Evaluation

- Four kinds of datasets provided. (Source point fixed at (0, 0, -28) [mm])
  - **Dataset A**: random-direction training sample (two datasets generated with different seeds: **A1** and **A2**)
    - random continuous directions => train model => Can the model learn continuous directions?
  - Dataset B: fixed-grid validation sample
    - fixed regular grid => monitor training and make resolution maps => Is the training stable and spatially uniform?
  - Dataset C: shifted-grid test sample
    - shifted fixed grid => test interpolation/generalization => Can the model interpolate to unseen fixed directions?
  - Dataset D: radial-ring stress-test sample
    - fixed-radius rings => test performance at large-radius boundary => Does the model degrade for large-angle directions?

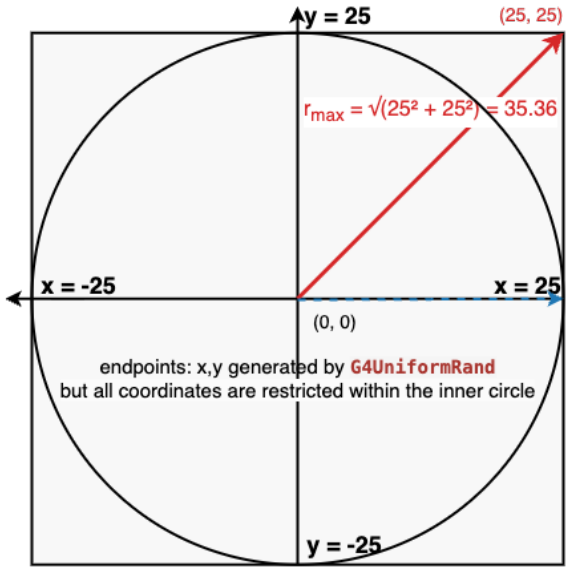

Endpoint plane: z = 0, 50 × 50

Dataset A: random training sample

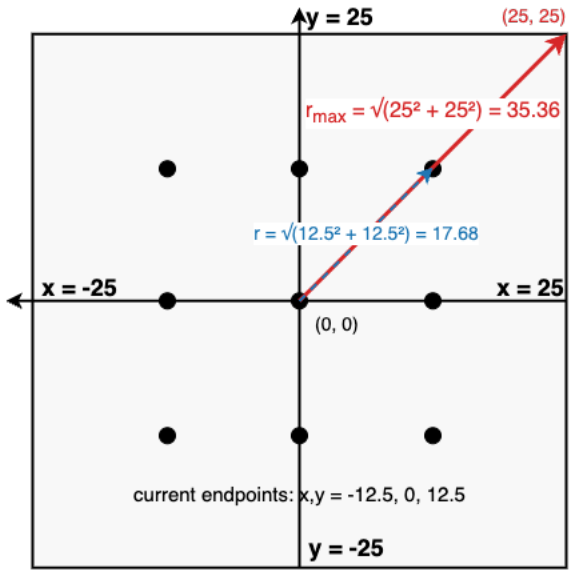

Endpoint plane: z = 0, 50 × 50

Dataset B: 3×3 regular grid

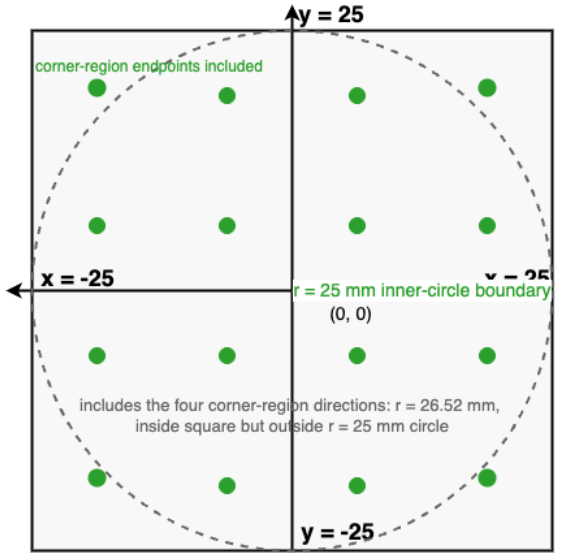

16 shifted endpoints: x,y = ±6.25, ±18.75, full 50 × 50 face

Dataset C: shifted-grid interpolation

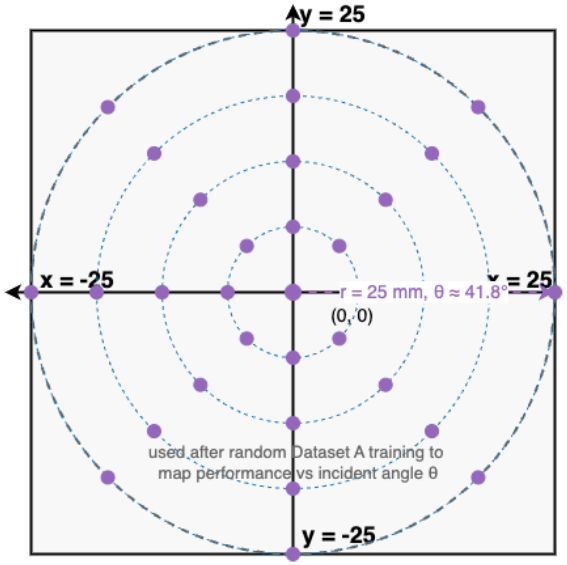

33 structured endpoints: center + r = 6.25, 12.5, 18.75, 25 mm rin

Dataset D: radial-ring test

MC Sample: Dataset A1 for Training

- 500k events simulated, yielding ~10k selected/effective events.
- Incident directions are randomly sampled from a fixed source point and cover the full detector entrance region.
- The endpoints are distributed inside a circle with R = 25 mm on the incident face.
- The 2D endpoint-density map and the r^2/ϕ distributions **confirm uniform directional sampling**.
- **Dataset A2** is generated with an independent random seed and used for cross-check / testing.

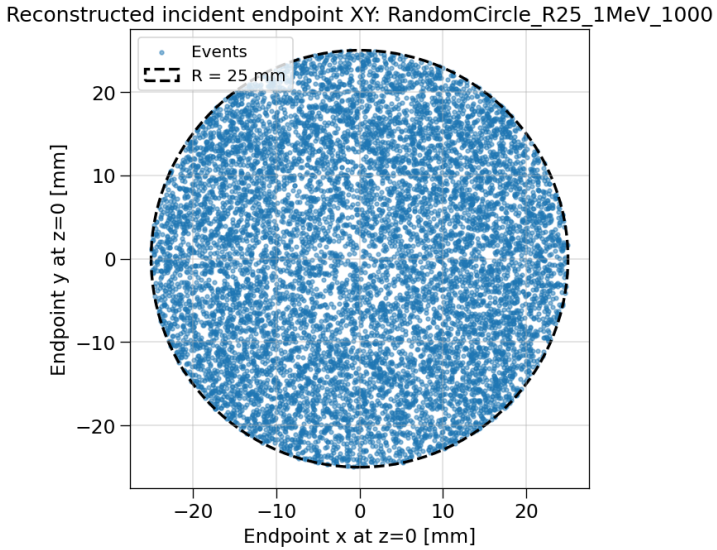

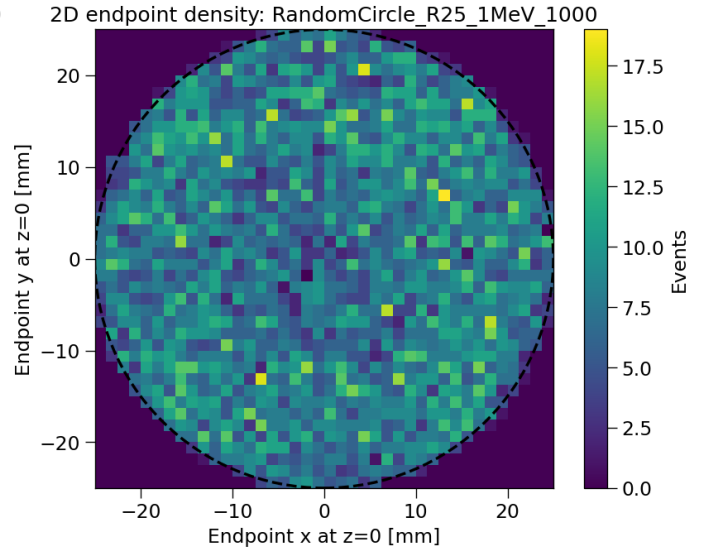

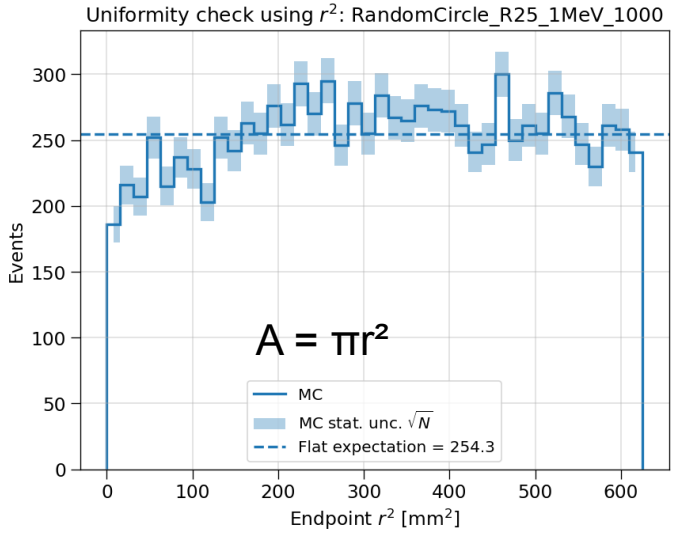

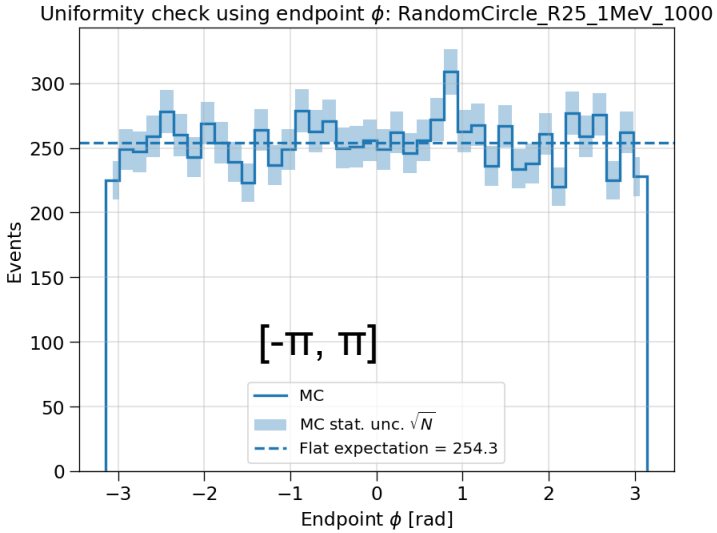

Dataset A1/A2 provide uniform random-direction samples for training and independent validation.

Pixelized Hits Position

- The SiPM hits positions are pixelized to match with $2\ \mathrm{mm} \times 2\ \mathrm{mm}$ pixel in real SiPM devices.

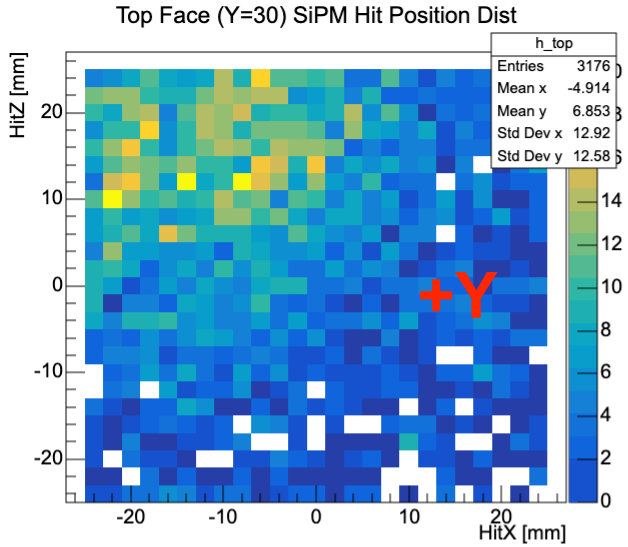

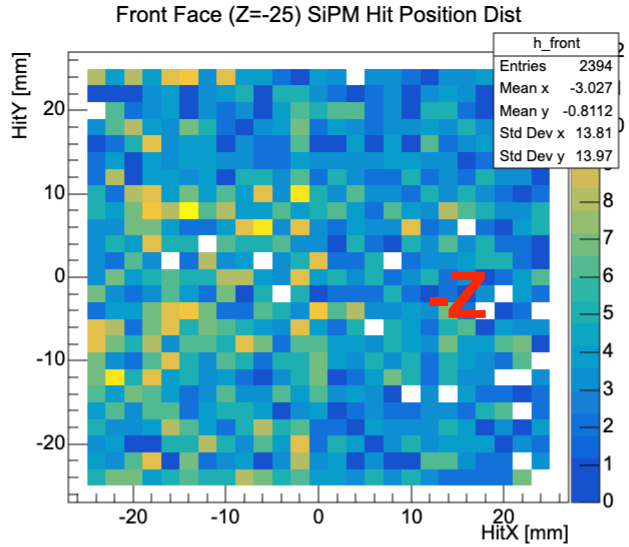

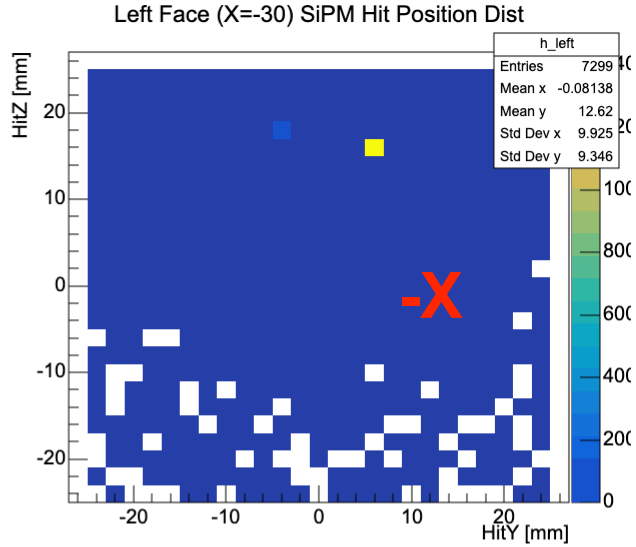

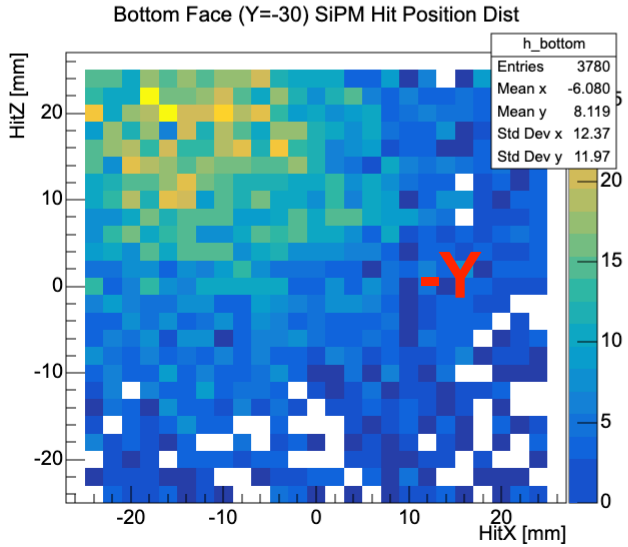

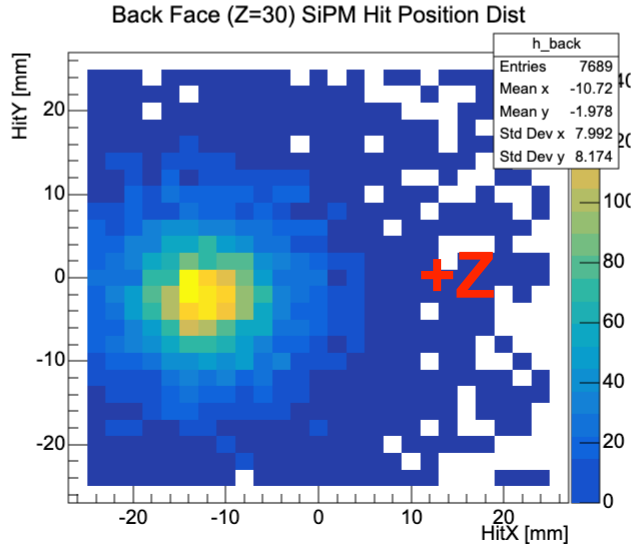

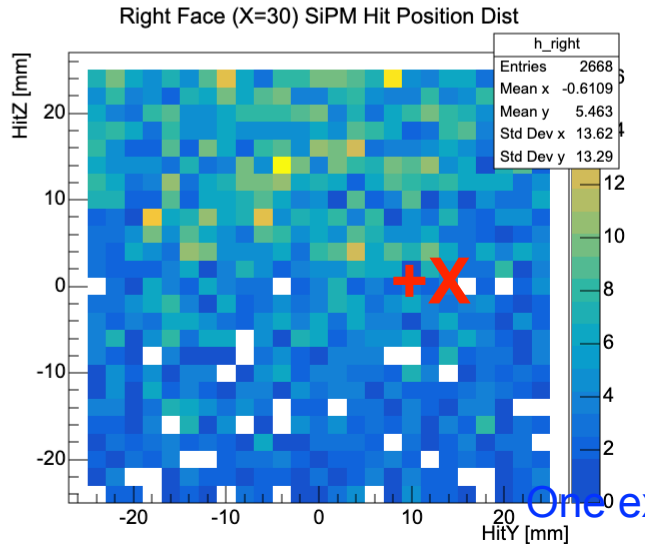

One example event

Multi-task Transformer Reconstruction

- Network: Transformer encoder extracts event-level information from photon-hit correlations.
- **Event input:** variable-length sequence of SiPM photon hits => x, y, z, E, t
- **Outputs**: four physical quantities are reconstructed simultaneously:
  - electron direction $\vec{u_e}$, electron energy E_e, scattered photon direction $\vec{u_{\gamma'}}$, incident gamma direction $\vec{u_\gamma}$
- Training: multi-task loss combines angular losses for directions and MSE loss for electron energy.
  - Direction: 3D unit vector and Energy: scalar
  - loss_direction = 1 - cos(predicted direction, true direction)
  - loss_energy = MSE(predicted E_e, true E_e)
  - task_weights = [0.3, 0.05, 0.3, 1.0]
- Training configuration:
  - n_splits = 4; shuffle = True; random_state = 42
  - batch_size = 2; epochs = 30; learning_rate =$1e^{-4}$
  - optimizer = AdamW; weight_decay = $1e^{-4}$
- Physics target:
  - Reconstruct the incident gamma-ray direction.

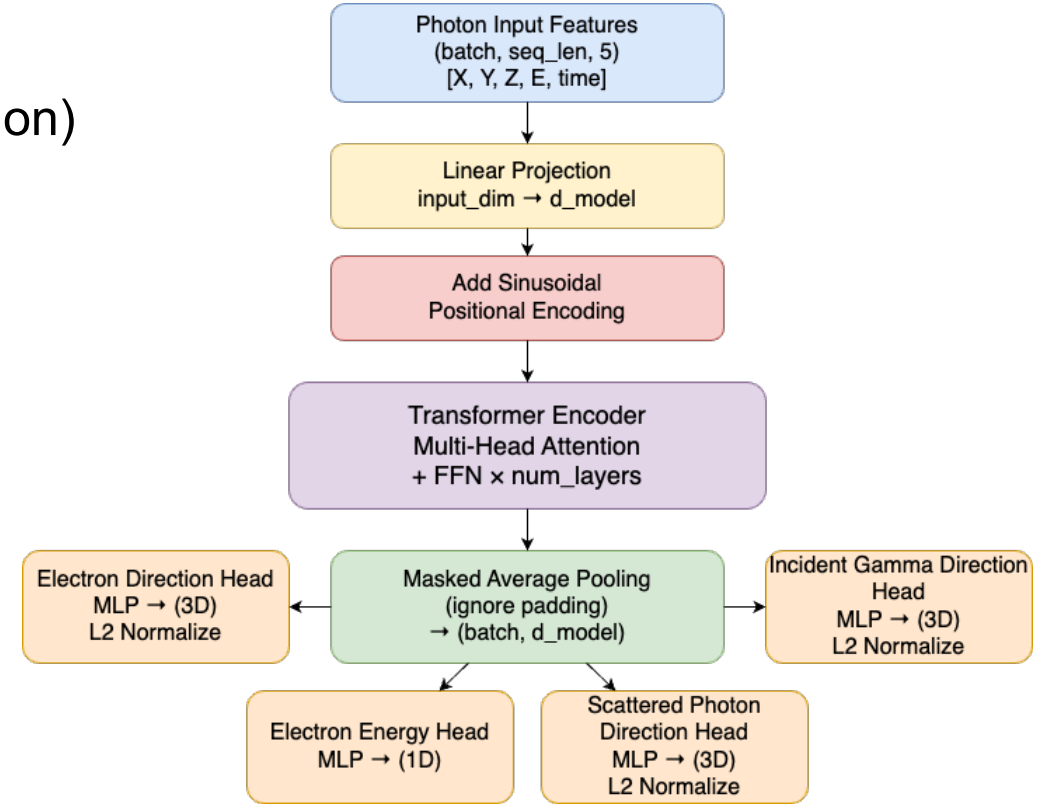

Training Setup and Results

- Four folds are applied for the cross-validation => four models were saved.
- 10174 events are split into four datasets: 75% for training and 25% for validation
- Currently, there are 30 epochs for the training in each fold.
- Since each event has 10^4 scintillation photons detected by SiPM, all ~10k events generate 10^8 photons and it is time-consuming to load all these photon variables.
  - Each epoch took 2 mins for the training using NVIDIA A800 GPU => total time: 4h.
- The training and validation loss curves in each fold were shown below.
  - Good convergence and stable performance.
- Apply the fourth model to other simulated datasets for the evaluations.

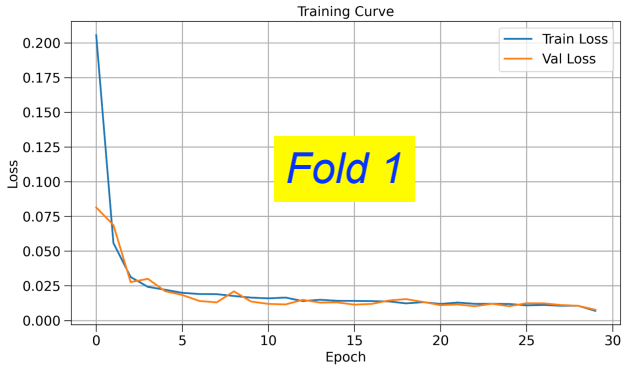

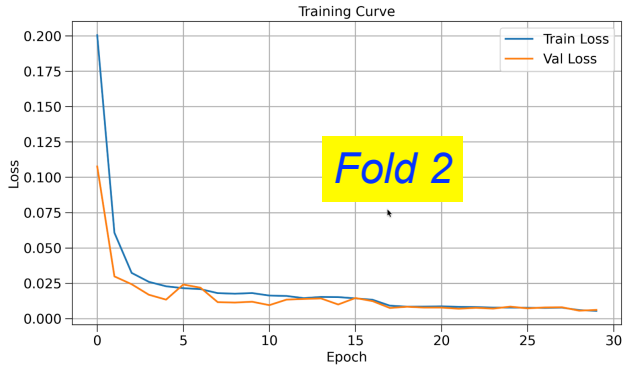

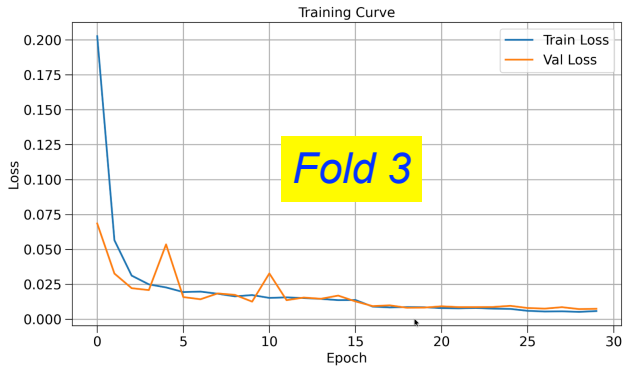

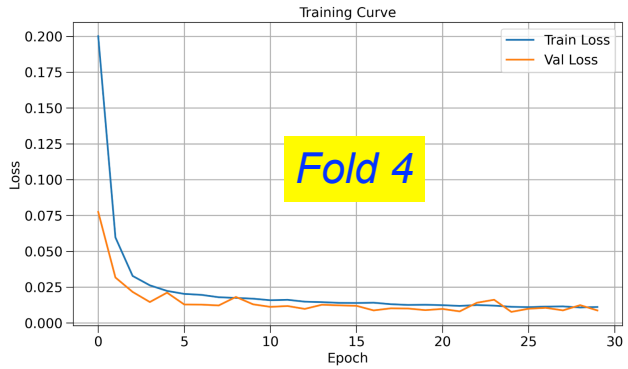

Evaluation Metrics for Reconstruction Performance

- How accurately does the model reconstruct the event-level Compton quantities, especially the incident gamma direction?
- Direction reconstruction performance
  - Compute opening-angle error between predicted and truth unit vectors: $\arccos(\hat{u}_{\text{pred}} \cdot \hat{u}_{\text{true}})$ in [0, π]
    - recoiled electron direction; scattered photon direction; incident gamma direction
  - Main reported metrics: mean, median, p68, p90
    - p68 is used as the main angular-resolution indicator.
    - p90 quantifies the non-Gaussian tail / containment performance.
- Energy reconstruction performance
  - Recoiled-electron energy residual:$(E_{\text{pred}} - E_{\text{true}})/E_{\text{true}} \times 100\,\%$
  - Report: mean, standard deviation, median, |p68|, |p90|

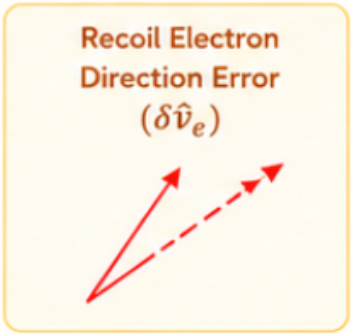

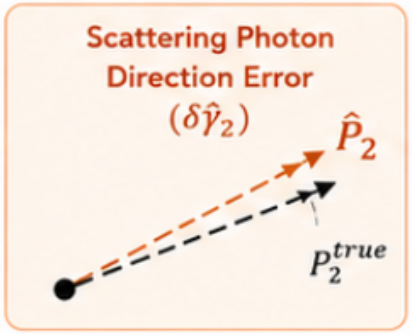

- Bias and stability checks
  - Signed θ and φ residuals: $\theta_{\text{pred}} - \theta_{\text{true}}$, $\varphi_{\text{pred}} - \varphi_{\text{true}}$
  - Local tangent-plane residuals: $\Delta\theta$ and$\sin(\theta_{\text{true}})\Delta\varphi$
  - Residuals versus incident θ and φ are checked to identify angular-dependent bias.

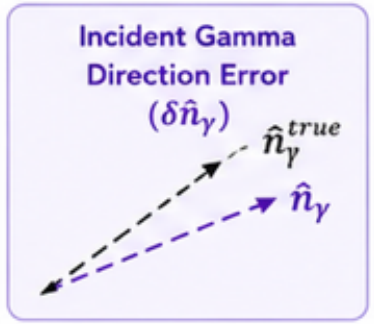

Preliminary Reconstruction Results: Dataset A2

Dataset A2: random incident directions from a fixed source point, tested on independent simulated events.

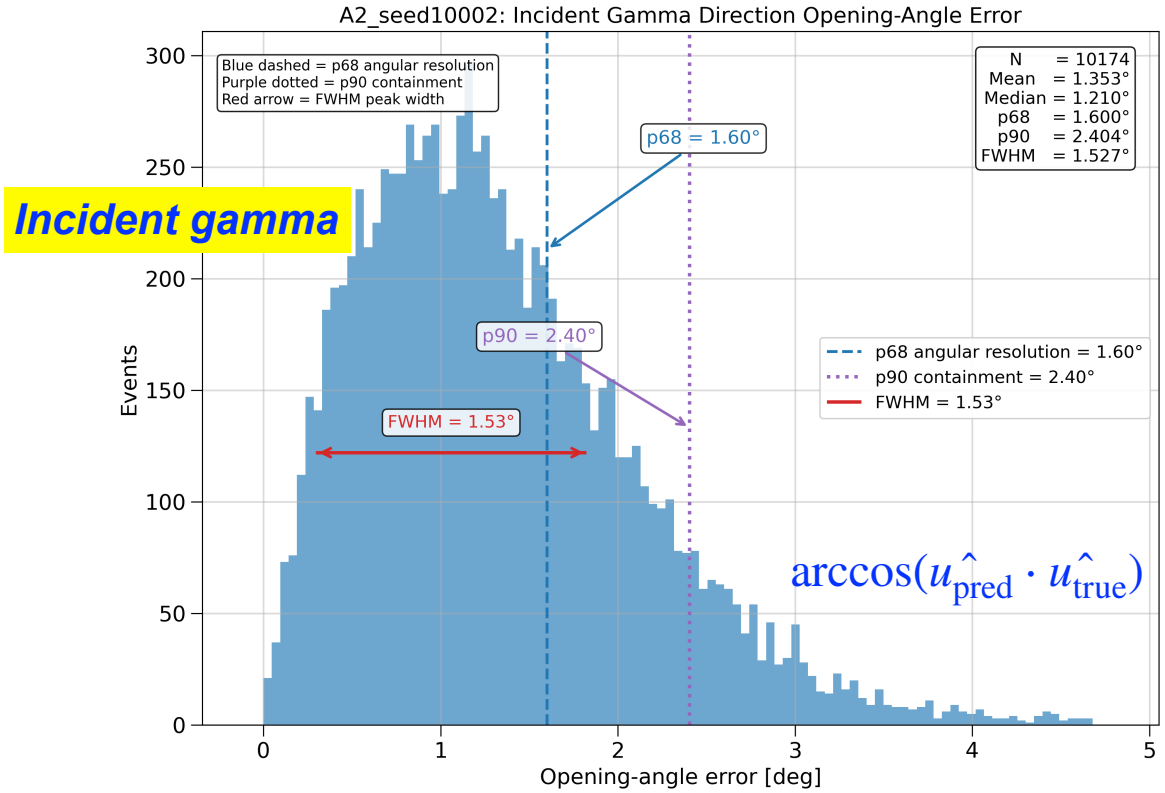

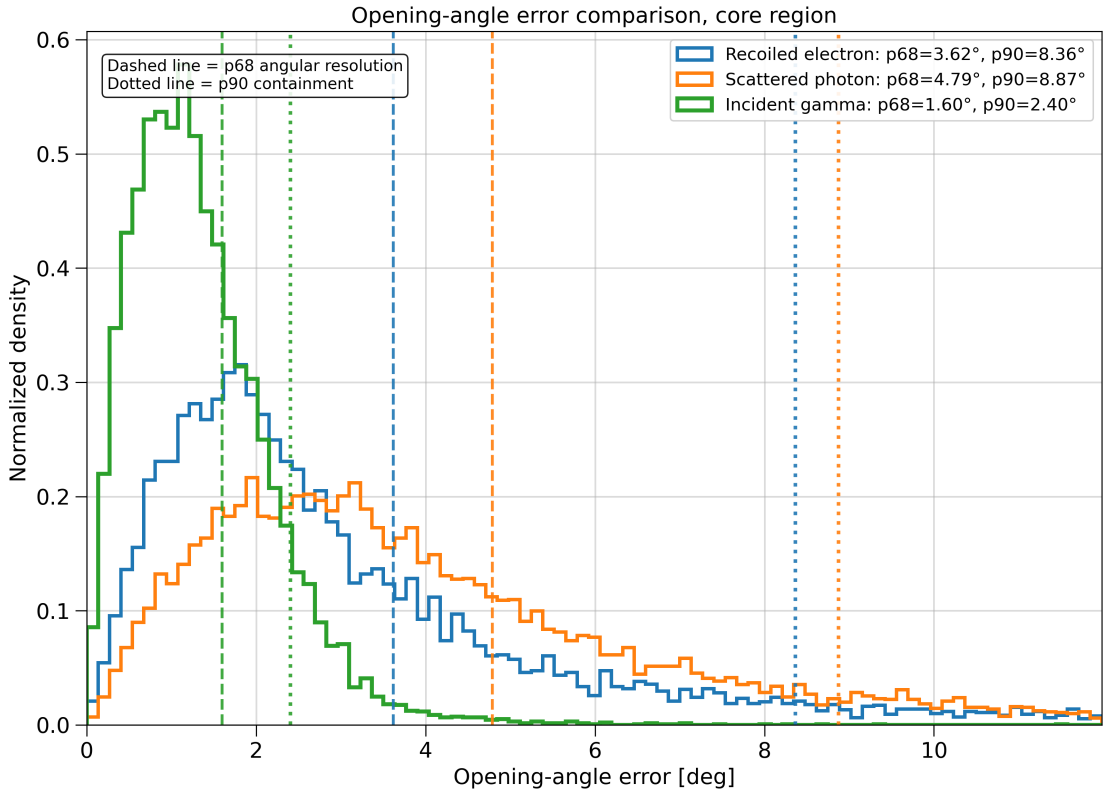

- Incident gamma angular resolution reaches p68 = 1.60°, with p90 containment = 2.40°.
- Multi-task reconstruction successfully learns the event topology from variable-length SiPM photon-hit sequences.
- The residual tail motivates further optimization of event selection, detector geometry, and training strategy.

Preliminary Reconstruction Results: Dataset A2

Dataset A2: random incident directions from a fixed source point, tested on independent simulated events.

Incident gamma

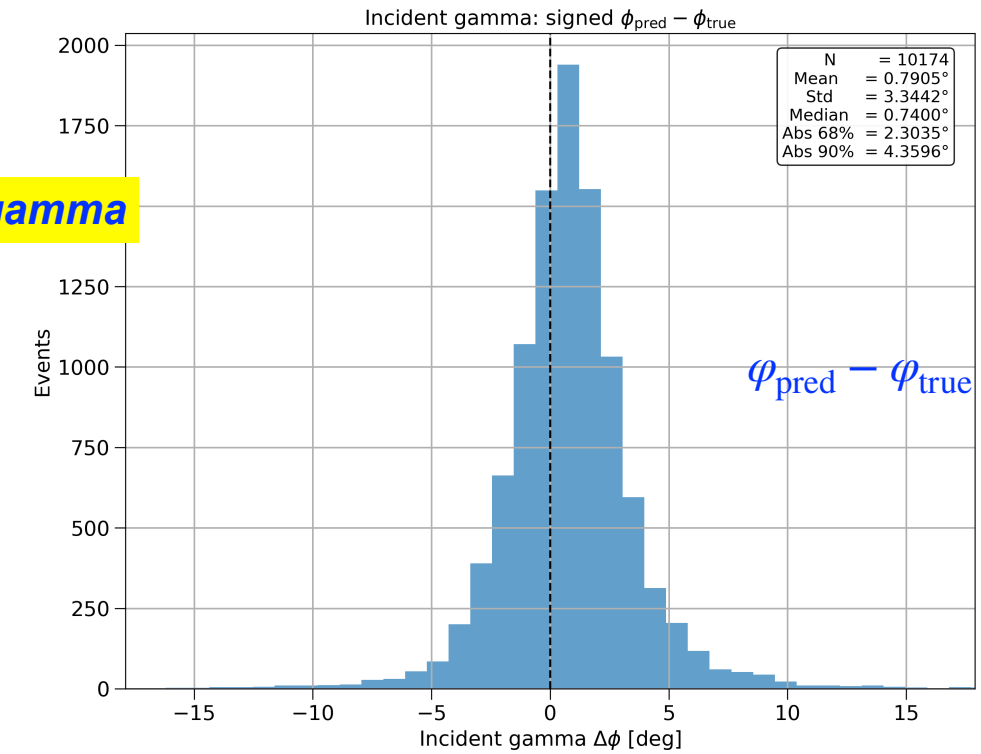

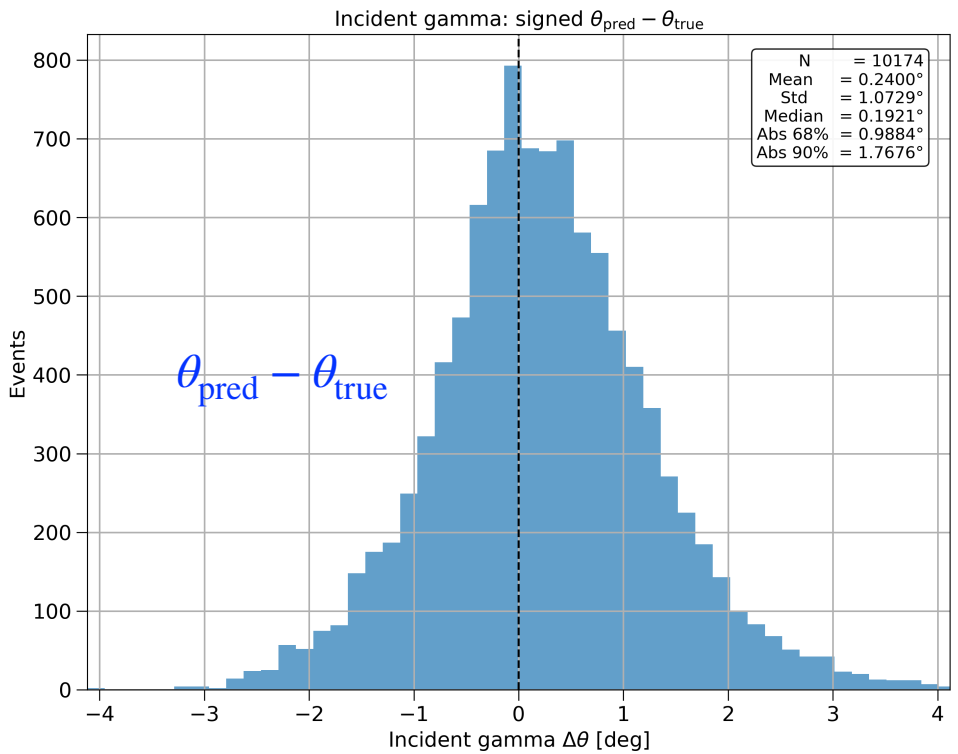

- Incident-gamma θ and φ residuals are centered near zero, showing limited directional bias.
- The θ residual is narrow, while the φ residual has a broader tail.
- The signed residuals support stable event-by-event incident-direction reconstruction.
- Remaining tails motivate improved event selection and detector-response calibration.

Preliminary Reconstruction Results: Dataset A2

Dataset A2: random incident directions from a fixed source point, tested on independent simulated events.

Recoil electron

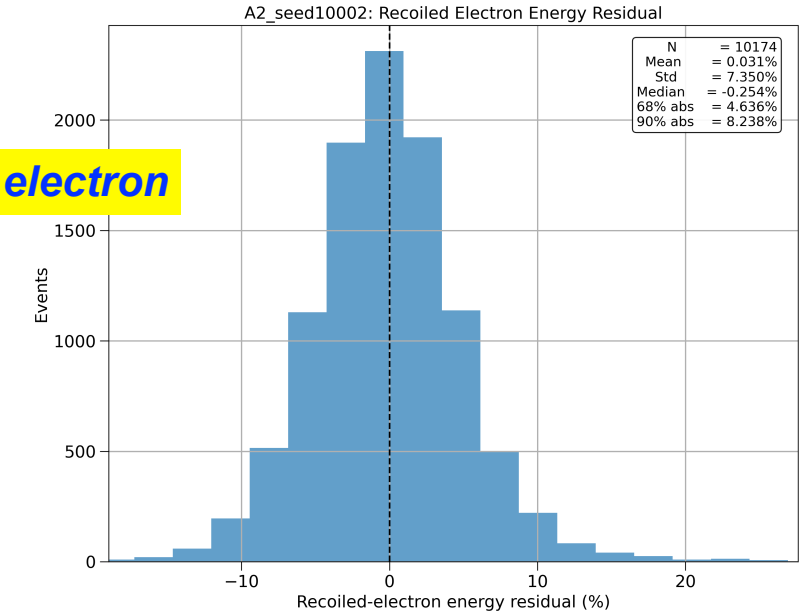

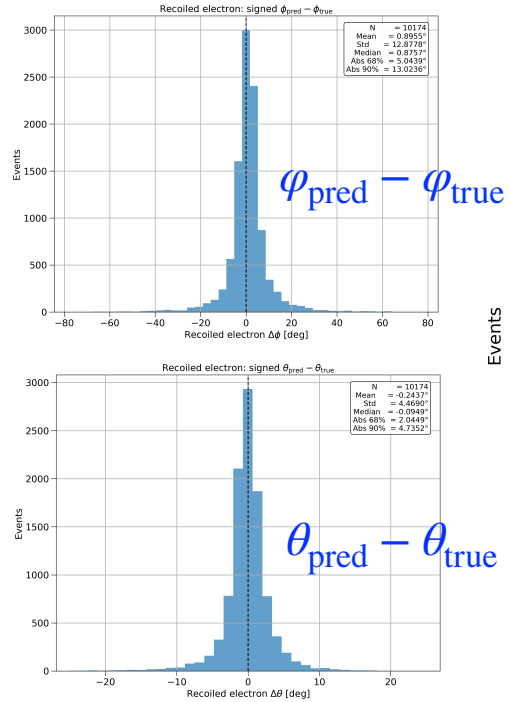

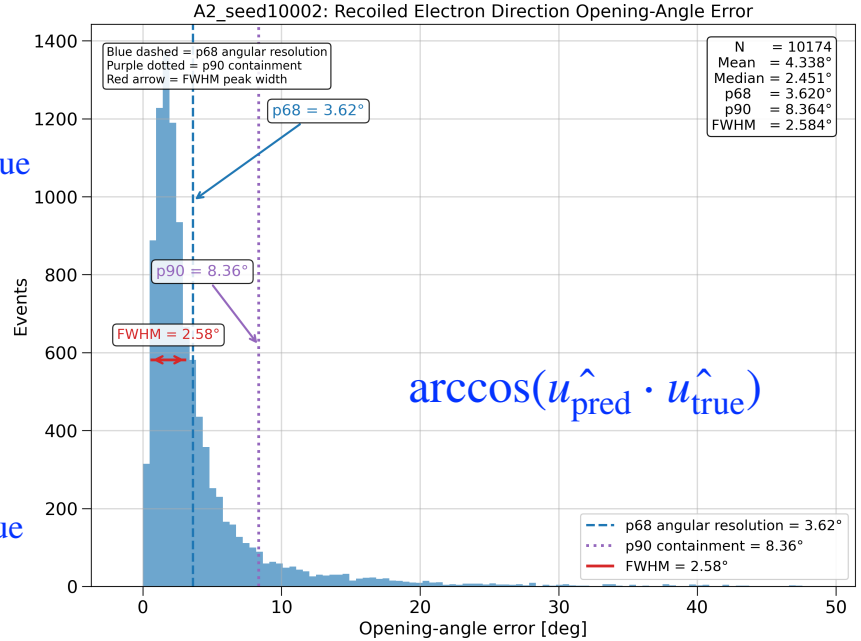

- Recoiled-electron energy shows good closure, with mean residual ≈ 0.03% and 68% absolute residual ≈ 4.64%.
- Signed θ and φ residuals are centered near zero, indicating limited angular bias.
- Recoiled-electron direction reaches p68 = 3.62° and p90 = 8.36°.
- Compared with incident-gamma reconstruction, the electron direction has a larger tail and remains a key target for further optimization.

Preliminary Reconstruction Results: Dataset A2

Dataset A2: random incident directions from a fixed source point, tested on independent simulated events.

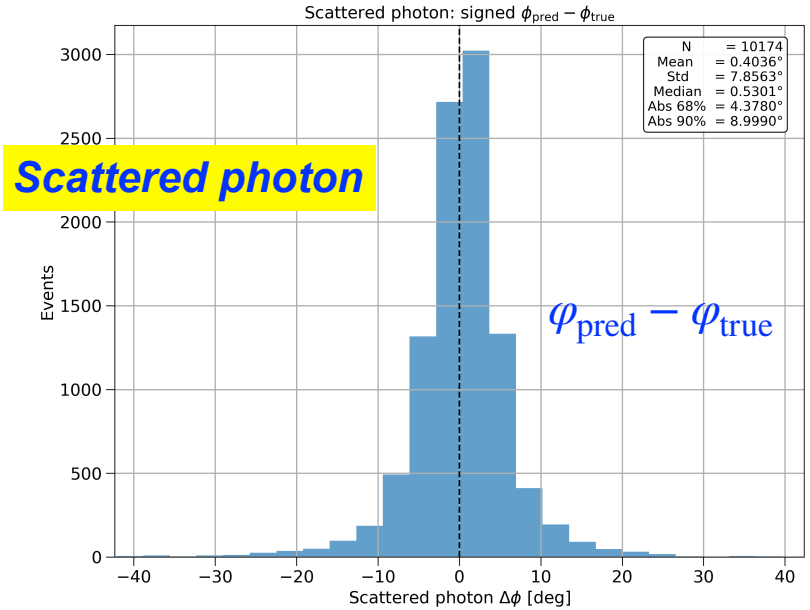

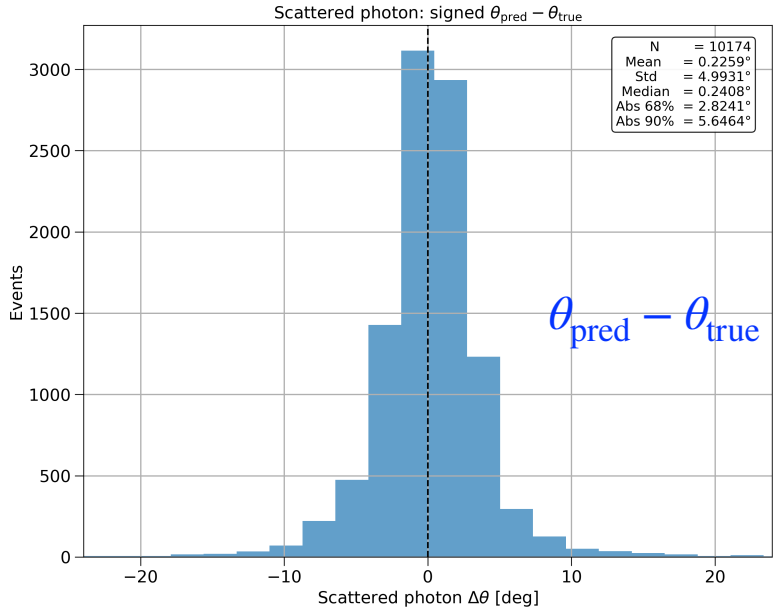

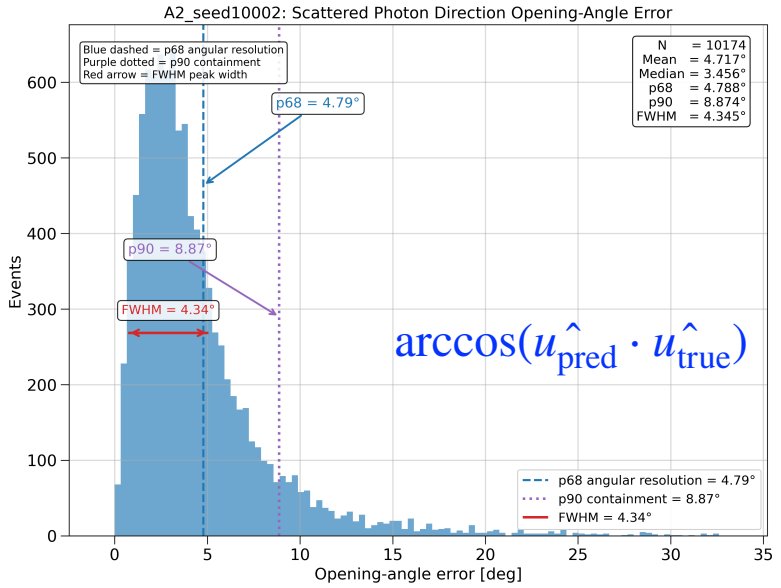

- Scattered-photon residuals are centered near zero, showing no strong directional bias.
- Direction reconstruction reaches p68 = 4.79° and p90 = 8.87°.
- The scattered-photon direction has a broader tail than the final incident-gamma direction.
- This motivates further optimization of intermediate-particle reconstruction and event-quality selection.

Preliminary Reconstruction Results: Dataset B

Dataset B: fixed nine-grid incident directions on the detector face, used to test direction-dependent reconstruction performance.

Incident gamma

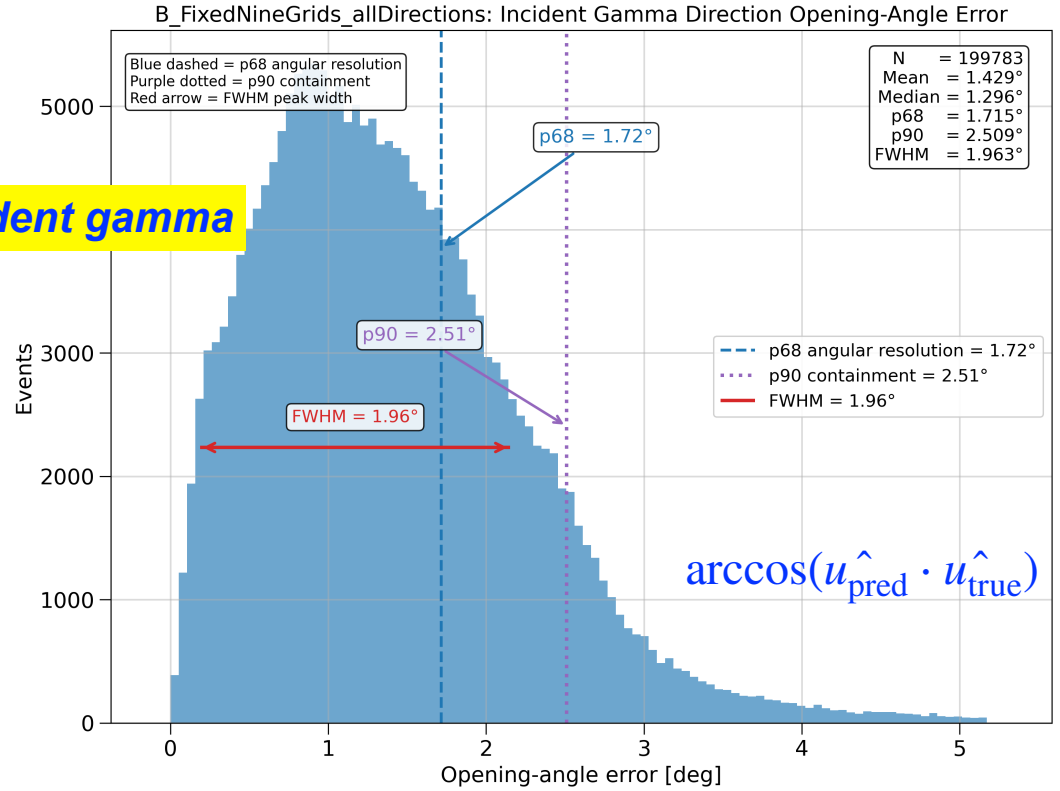

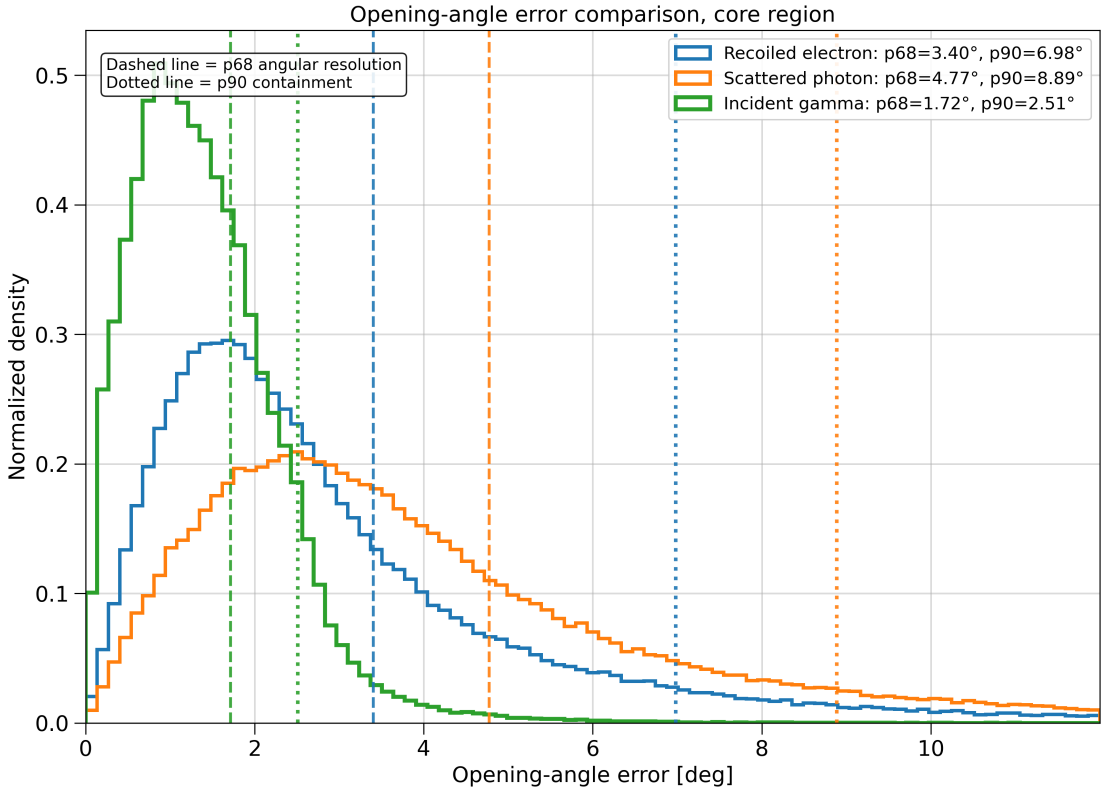

- Incident gamma angular resolution reaches p68 = 1.72°, with p90 containment = 2.51°.
- The incident gamma direction shows the best angular performance among the three reconstructed targets.
- Multi-task reconstruction successfully learns the event topology from variable-length SiPM photon-hit sequences.
- The residual tail motivates further optimization of event selection, detector geometry, and training strategy.

Preliminary Reconstruction Results: Dataset C

Dataset C: shifted-grid incident positions on the detector face, providing an interpolation test between the fixed-grid directions used in Dataset B.

Incident gamma

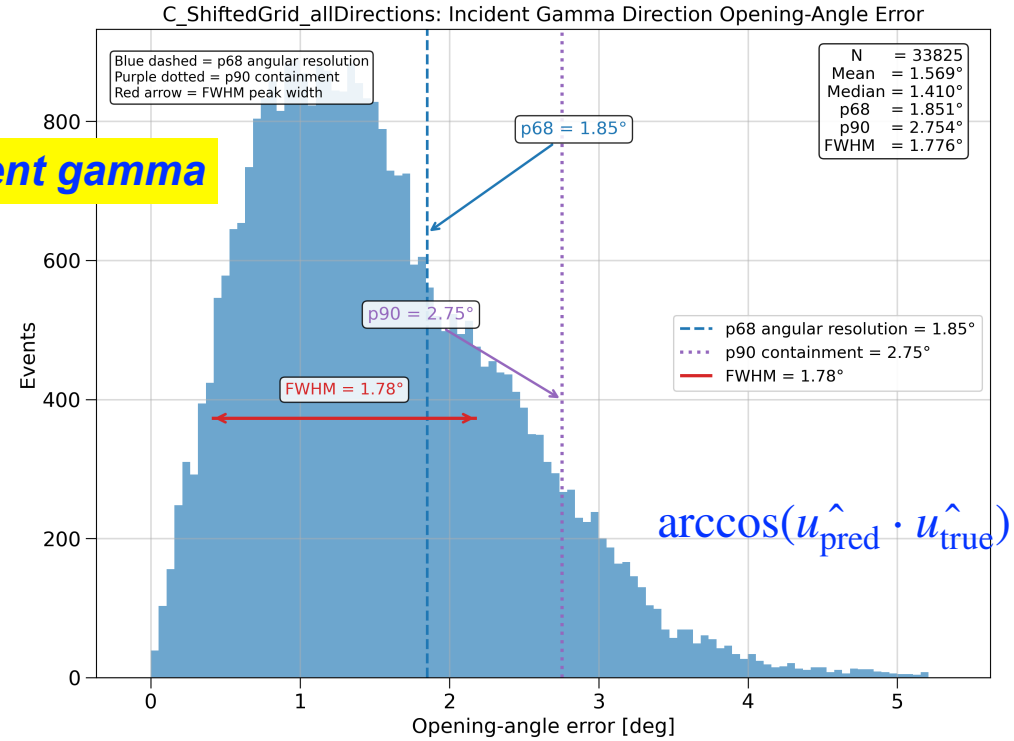

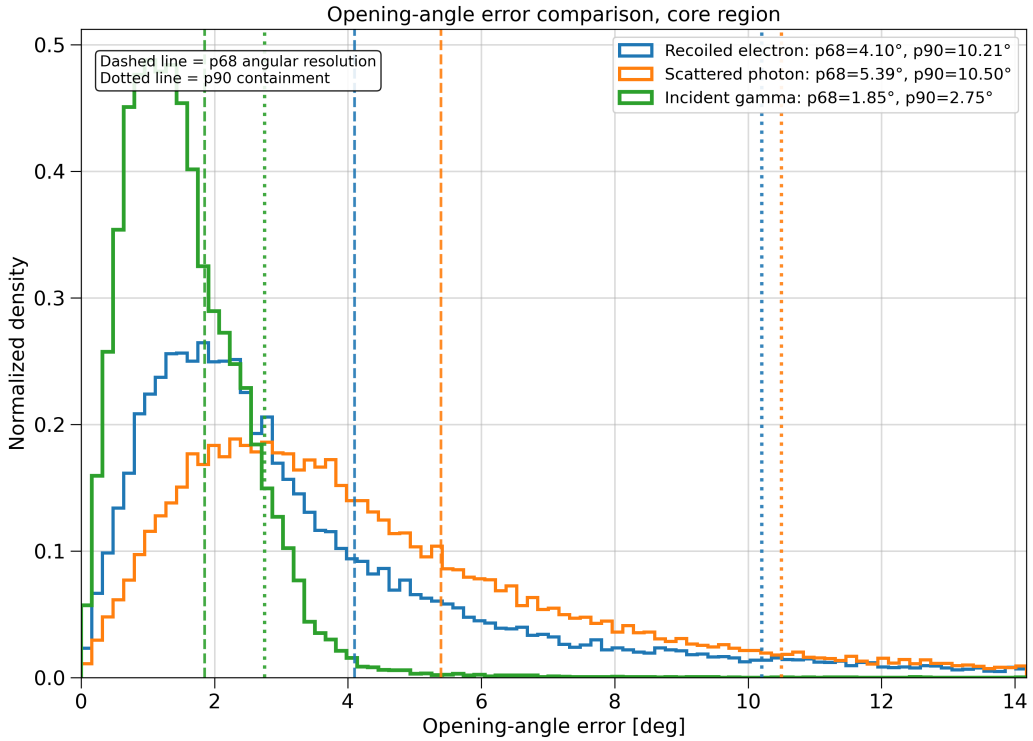

- Dataset C evaluates interpolation to shifted-grid incident positions.
- Incident gamma angular resolution reaches p68 = 1.85°, with p90 containment = 2.75°.
- The incident gamma direction remains the most accurately reconstructed quantity.
- The residual tail and slight performance degradation motivate improved angular coverage, event selection, and training strategy.

Preliminary Reconstruction Results: Dataset D

Dataset D: radial-ring incident positions on the detector face, used to test radial dependence and direction-dependent reconstruction robustness.

Incident gamma

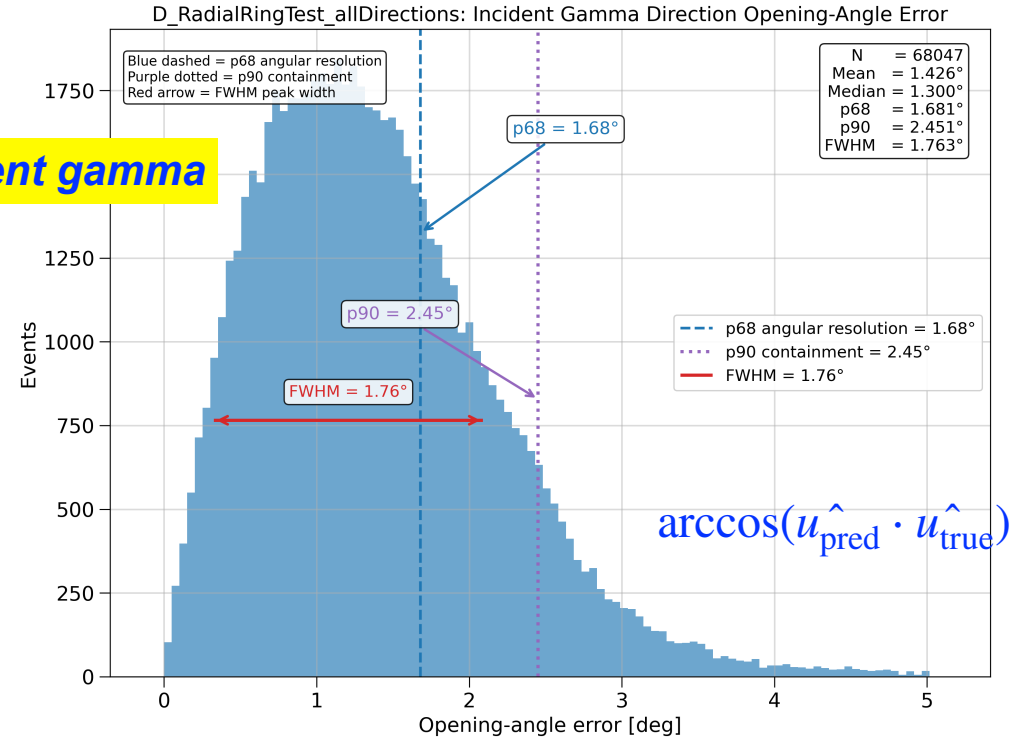

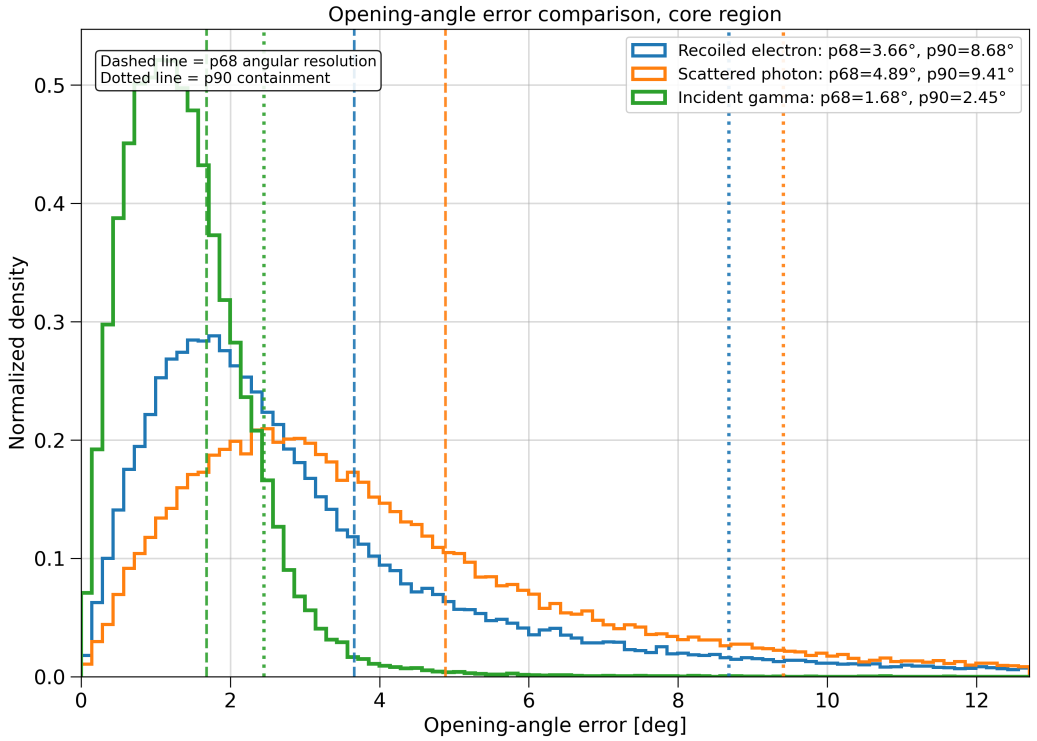

- Dataset D tests radial-position dependence using ring-like incident positions on the detector face.
- Incident gamma angular resolution reaches p68 = 1.68°, with p90 containment = 2.45°.
- The incident gamma direction remains the best-reconstructed quantity among the three targets.
- The residual tail motivates further optimization of event selection, photon statistics, and detector-geometry coverage.

Summary of Preliminary Reconstruction Results

- Stable incident gamma reconstruction is achieved across multiple incident-direction configurations.
- The angular resolution is consistently p68 ≈ 1.6°–1.9°, with p90 containment ≈ 2.4°–2.8°.
- The shifted-grid sample shows a modest degradation, indicating that interpolation to unseen incident positions is more challenging.
- These preliminary results demonstrate the feasibility of Transformer-based event-level Compton imaging with SiPM photon-hit information.

Dataset	Incident-position setup	Incident gamma p68	Incident gamma p90	Purpose
A2	Random incident directions	1.60°	2.40°	Random-direction test
B	Fixed nine-grid directions	1.72°	2.51°	Direction-dependent validation
C	Shifted-grid directions	1.85°	2.75°	Interpolation/generalization test
D	Radial-ring directions	1.68°	2.45°	Radial-dependence test

Why this detector concept?

Technology	Main idea	Key limitation	Relevance to this work
Mechanical collimation	Uses a mask/collimator to select photon direction	Very low efficiency at MeV energies	Avoid mechanical photon blocking
Coded aperture / coded collimation	Reconstructs image from mask shadow pattern	Requires accumulated statistics; mask still blocks photons	This idea targets event-level reconstruction
Traditional Compton camera	Uses interaction positions and energies to form a Compton cone	Single-event direction is ambiguous	This work aims to reduce cone ambiguity
Electron-tracking Compton camera	Measures recoil-electron track with silicon/TPC	Complex, bulky, expensive	This work avoids conventional tracking layers
Hybrid Cherenkov–scintillation detector	Uses optical topology to infer Compton event information	New concept; needs realistic validation	Compact event-level MeV gamma reconstruction

Detector: compact optical-readout architecture based on a CsI(Tl) scatterer, BGO absorbers, and SiPM arrays

The proposed detector targets the gap between traditional Compton cameras and electron-tracking Compton cameras: event-level direction reconstruction without conventional tracking hardware.

Where does our method currently stand, and what is still needed?

Performance Item	Reference/MeVGRO Targets	Current Status of This Work
Energy range	0.3~3MeV(100MeV) (8keV~3MeV for CBM)	targets 1–10 MeV, with current preliminary results at 1 MeV.
FOV	3.6 sr (±65°), Imaging	Currently simulated ±83°
Angular resolution	~2°@1MeV, 100MeV (FWHM)	incident gamma p68 opening-angle error: about 1.6°–1.9° at 1 MeV
Effective area	~1000cm2@1MeV, 100MeV (3σ)	Not yet quantified
Energy resolution	<1%@662keV(by CZT)	Not yet fully evaluated

The current result is a **promising proof-of-principle selected-event study**. A full comparison with state-of-the-art MeV instruments requires efficiency, effective area, energy resolution, FOV, background rejection, and sensitivity studies.

Summary and Conclusions

- Proposed a compact hybrid Cherenkov–scintillation Compton-camera concept: CsI(Tl) scatterer + BGO absorbers + SiPM optical readout.
- Developed a “soft electron-tracking” approach: recoil-electron direction is inferred from Cherenkov–scintillation optical topology, avoiding conventional silicon/TPC tracking layers.
- Applied a multi-task Transformer to variable-length SiPM photon-hit sequences: reconstructing electron direction, electron energy, scattered-photon direction, and incident-gamma direction.
- Achieved promising selected-event performance at 1 MeV: incident-gamma p68 ≈ 1.6°–1.9° across random, grid, shifted-grid, and radial-ring test samples.
- This is a proof-of-principle detector-level simulation.
  - Full comparison with state-of-the-art MeV instruments requires energy resolution, detection efficiency, effective area, FOV, background rejection, and sensitivity studies.

Optical photon topology (Cherenkov) can provide electron-direction information, enabling compact event-level Compton reconstruction without a conventional tracker.

Hybrid Compton Camera: Detector Layout

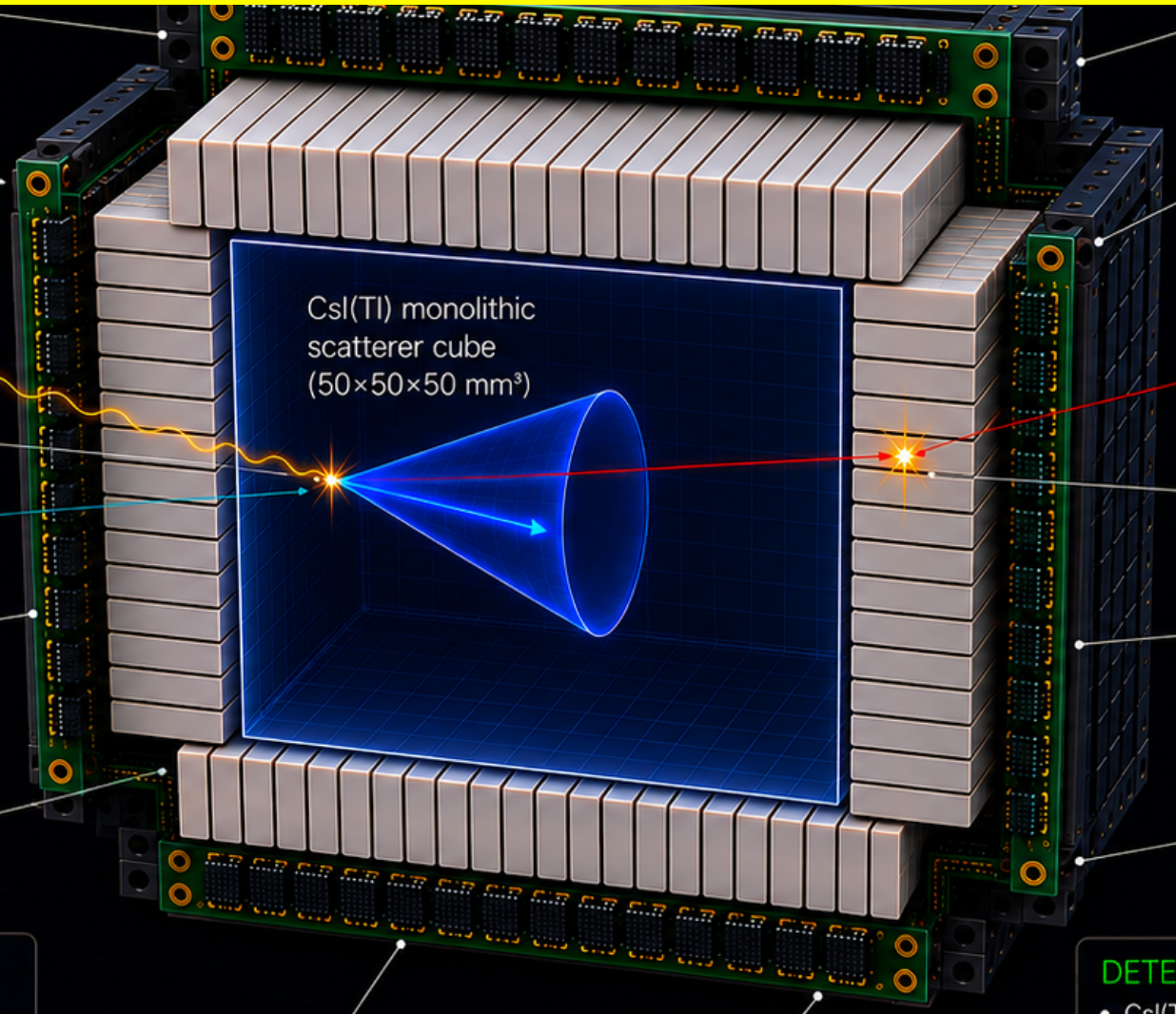

SiPM array (25×25 channels) for +Y face readout

BGO scintillator bars (25×25 array) individually wrapped with Teflon (+Y face)

Incident gamma ray (~MeV)

Compton scatter interaction

Cherenkov light cone from recoil electron

BGO scintillator bars (25×25 array) individually wrapped with Teflon (+X face)

SiPM array (25×25 channels) for +X face readout

SiPM array (25×25 channels) for +Z face readout

BGO scintillator bars (25×25 array) individually wrapped with Teflon (+Z face)

Scattered gamma ray absorbed in BGO

Scintillation light in BGO bar

BGO scintillator bars (25×25 array) individually wrapped with Teflon (−X face)

SiPM array (25×25 channels) for −X face readout

SiPM array (25×25 channels) for −Y face readout

SiPM array (25×25 channels) for −Z face readout

BGO bar (individually wrapped with Teflon)

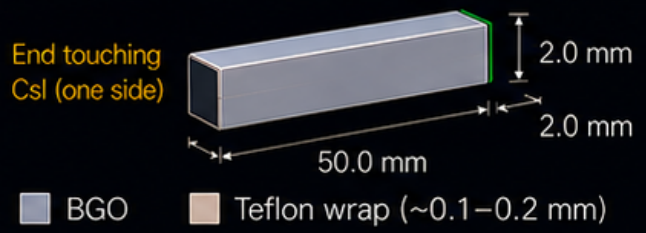

DETECTOR FEATURES

- CsI(Tl) cube: 50×50×50 mm³ (monolithic)
- BGO bars: 2.0×2.0×50.0 mm³ (25×25 per face, 5 faces)
- Each BGO bar wrapped with Teflon reflector
- SiPM arrays (25×25) with 90° routing to cover BGO readout
- Five-side readout: +X, −X, +Y, −Y, +Z
- CsI and BGO ends tightly close (no gap)

An image on the detector geometry and technology descriptions from ChatGPT

Thanks for your attention!

Email Address: qiuping.shen@cern.ch

Backup Slides

Proposed Detector Concept and Principle

- From energy conservation and Compton kinematics:

$$E_\gamma = E_e + E'_\gamma, \qquad \cos\theta = 1 - m_e c^2 \left(\frac{1}{E'_\gamma} - \frac{1}{E_\gamma} \right)$$

  - Conventional **Compton camera**s use only energy and interaction positions, so one event gives a **Compton cone** rather than a unique source direction, or requiring heavy silicon-based tracker.

- Basic detector and reconstruction principle:
  - A MeV incident gamma ray first undergoes Compton scattering in the CsI(Tl) scatterer, producing a recoil electron and a scattered photon.
    - The recoil electron deposits energy in the CsI(Tl), giving E_e and the first interaction position P_1.
    - In CsI(Tl), the recoil electron produces two complementary optical signals:
      - Cherenkov light: prompt (ps-scale) emission, directional, sensitive to electron direction.
      - Scintillation light: slower (~1 μs), nearly isotropic, useful for energy and position reconstruction.
    - The scattered photon is absorbed in the BGO absorber, giving E'_γ and the second interaction position P_2.
    - SiPM arrays: measure optical photon-hit position, timing, charge/amplitude, providing the full event topology.
- **New detector concept**: infer recoil-electron direction from Cherenkov–scintillation optical topology, enabling single-event Compton reconstruction without relying on silicon tracking layers.

BGO Energy Leakage to CsI(Tl)

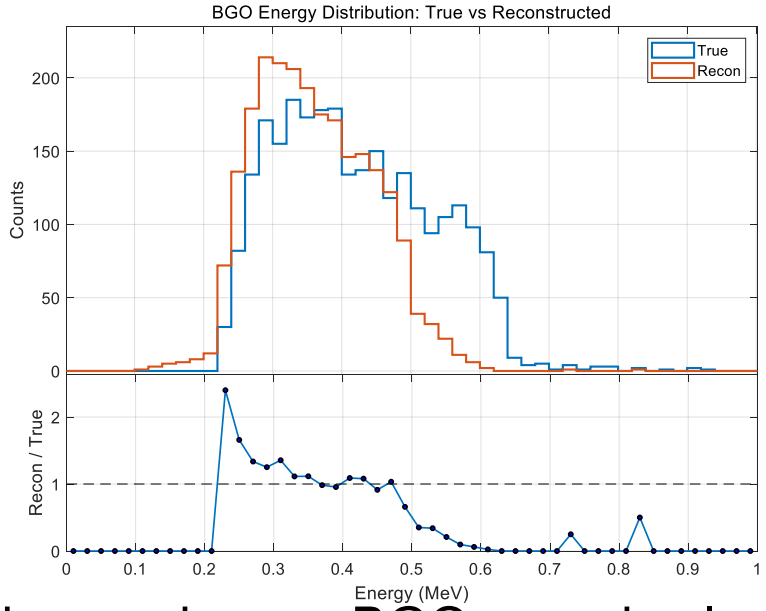

- Observed some BGO energies leaking to the CsI(Tl).
  - 200keV to 700 keV
- Using electrons with varied energies starting from the center of BGO and then counting the photons for the brightest pixel and total photons.
  - Taking the ratio as the leakage SF

BGO CsI(Tl) **Baseline Geometry**

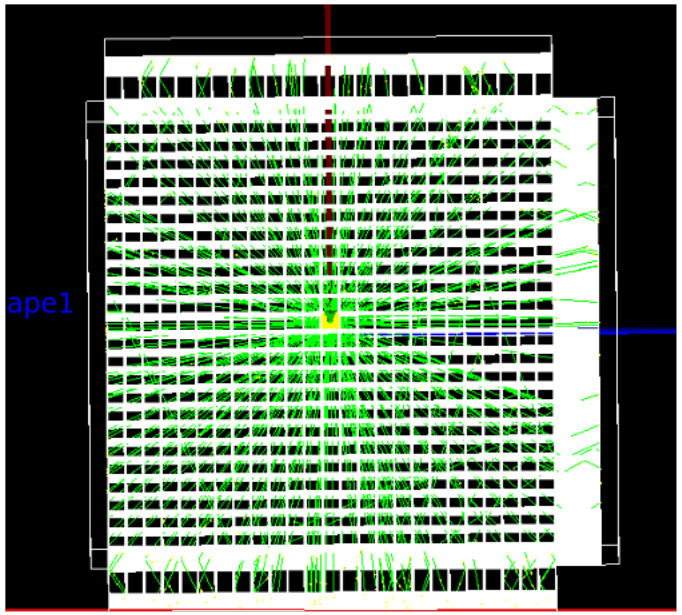

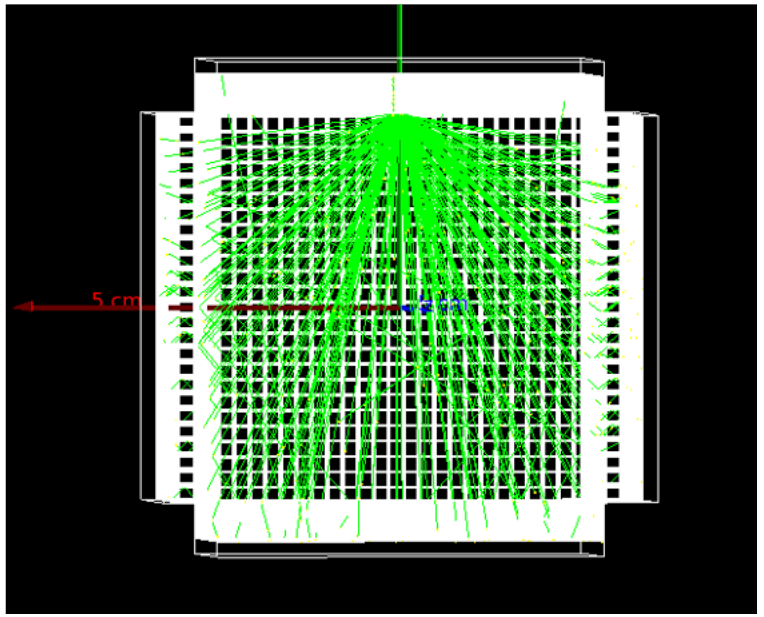

Energy/MeV	Brightest Pixel	Total Photons	Leakage SF
200	776	997	1.285
300	1121	1426	1.272
400	1561	2000	1.281
500	1960	2531	1.291
600	2209	2844	1.287
700	2699	3436	1.273

Investigations on BGO Shape

- New idea: replace the flat BGO end with a tapered tip to guide photons through total internal reflection.
- BGO: bar with 4mmx2mmx2mm and taper with square 0.2mmx0.2mm, length: 1mm
- The Teflon wrapper geometry is kept unchanged to isolate the effect of the BGO shape.

Baseline Geometry

Trapezoid:

To construct a **trapezoid** use:

```
G4Trd(const G4String& pName,
            G4double  dx1,
            G4double  dx2,
            G4double  dy1,
            G4double  dy2,
            G4double  dz)
```

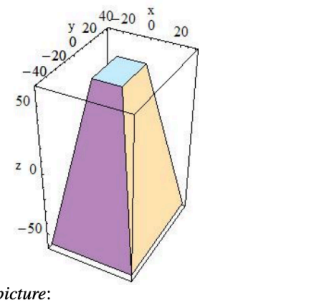

In the picture:
dx1 = 30, dx2 = 10, dy1 = 40, dy2 = 15, dz = 60

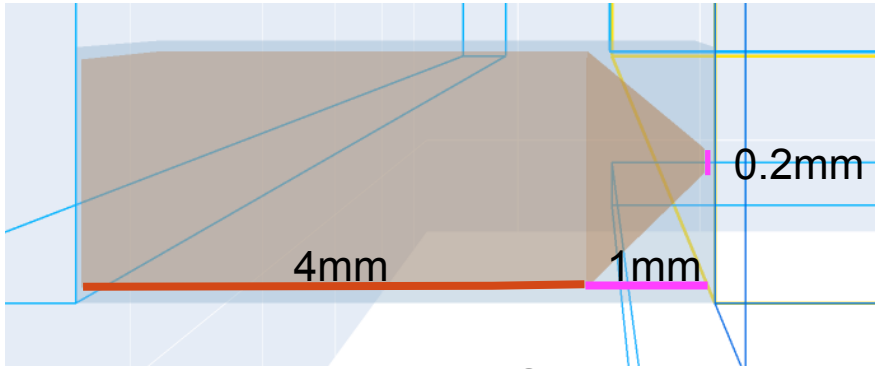

New Geometry

Next step: will perform further simulation studies on new geometry to evaluate.

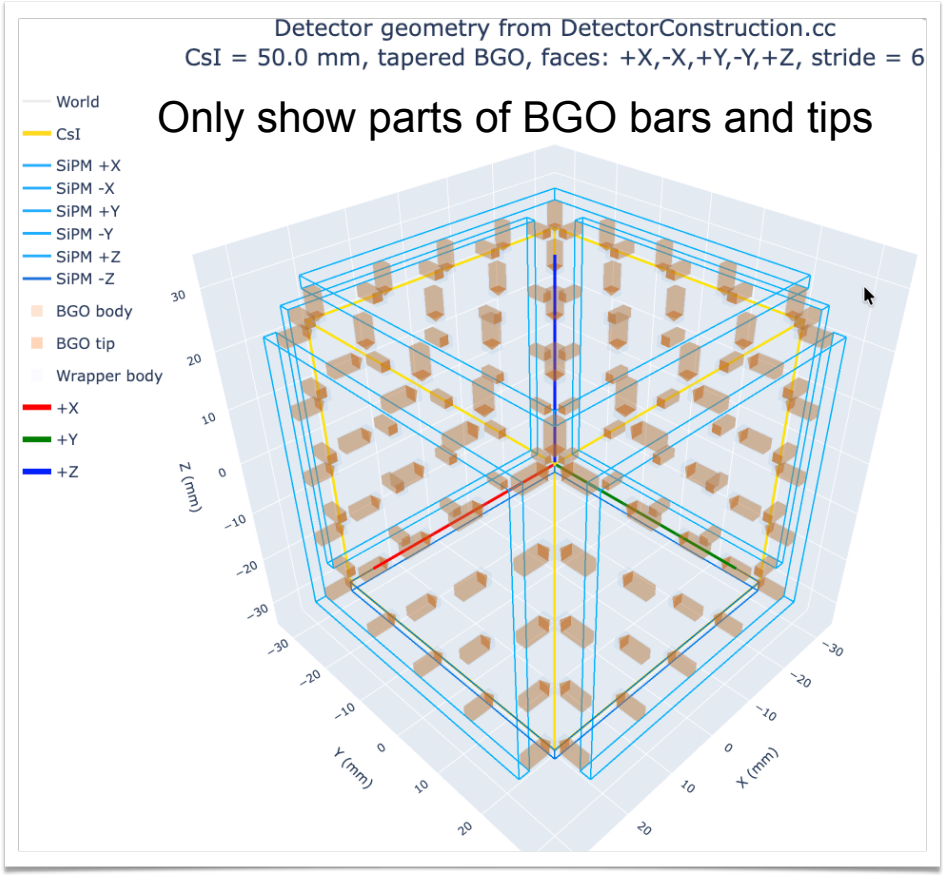

Research Background

1. Mechanical collimation

Simple and widely used, but suffers from very low detection efficiency; spatial resolution and sensitivity cannot be optimized simultaneously.

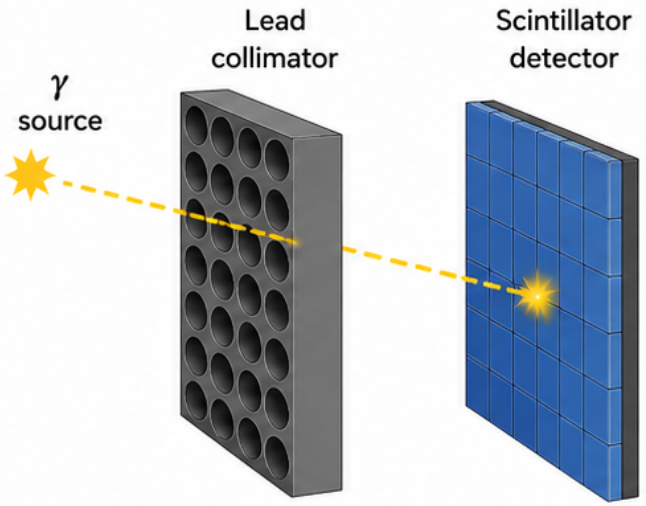

Schematic images from ChatGPT

- Simple structure, mature technology
- Very low detection efficiency (most photons are blocked)
- Spatial resolution and sensitivity cannot be optimized simultaneously

2. Traditional Compton camera without electron direction

Reconstructs a Compton cone from energy and position measurements, but single-event source direction remains ambiguous and requires many events for image formation.

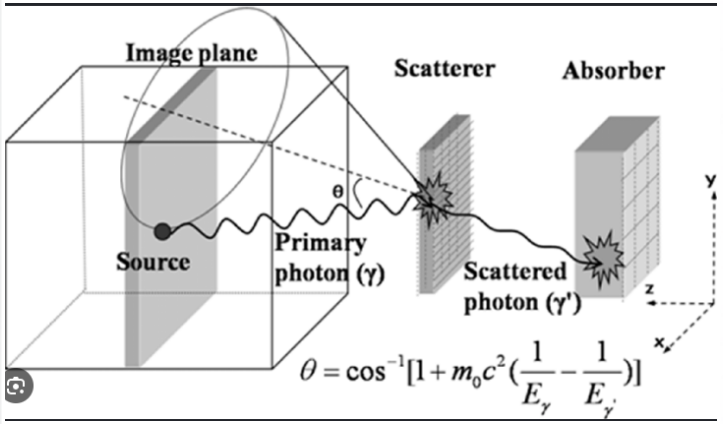

- Higher efficiency than mechanical collimation
- Cone ambiguity: source lies somewhere on the cone
- Single-event direction is ambiguous, requires many events for imaging

3. Electron-tracking Compton camera

Can reduce cone ambiguity by measuring recoil-electron direction, but usually requires complex silicon tracking layers or bulky TPC systems, increasing detector size, cost, and readout complexity.

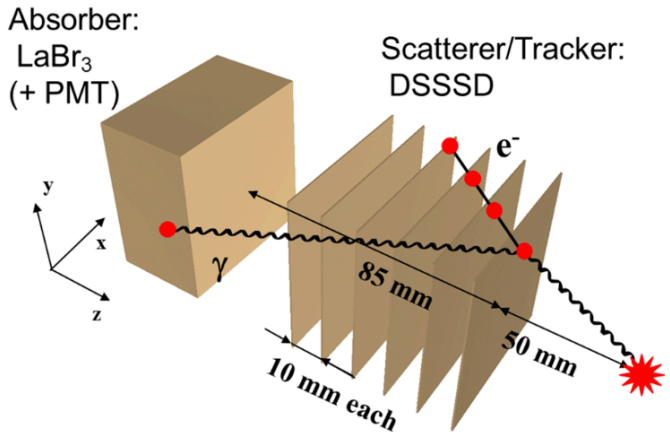

epjconf_inpc2013_11036.pdf

- Reduces cone ambiguity with electron direction information
- Requires complex silicon tracking layers or bulky TPC systems
- Larger size, higher cost, more complex readout

Principle Visualization

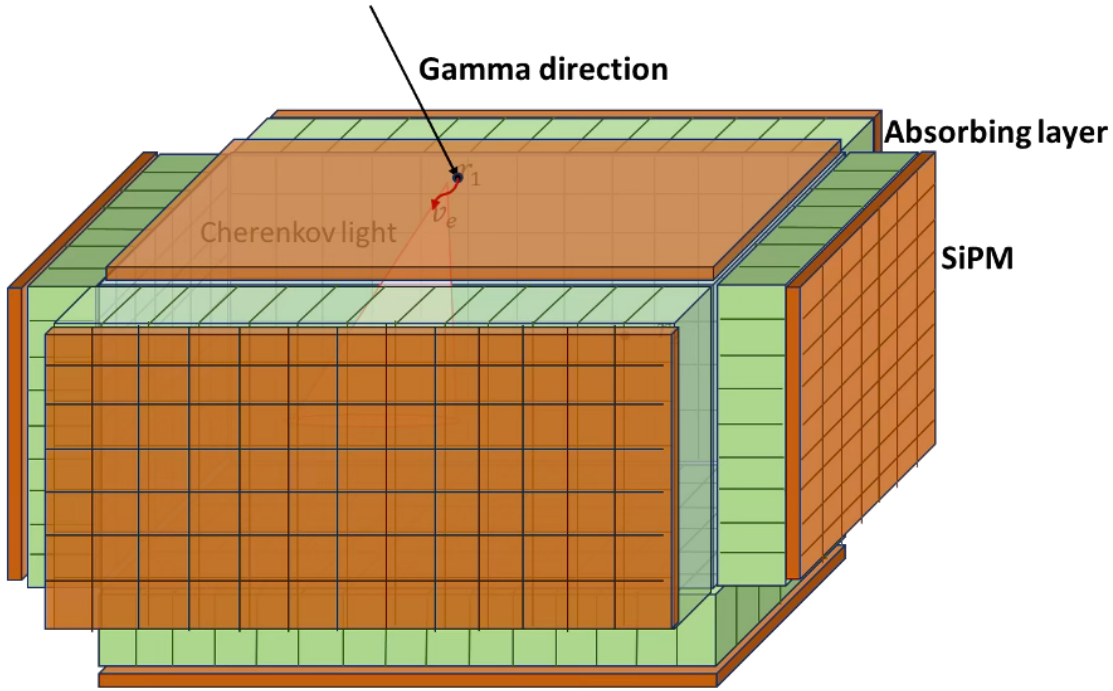

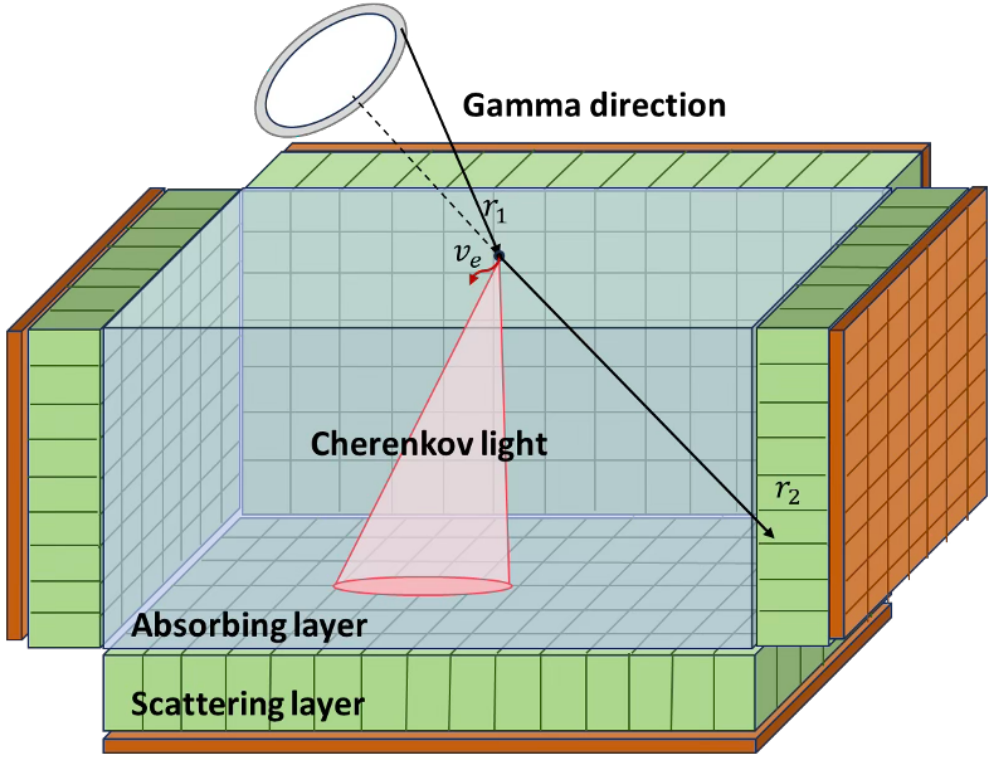

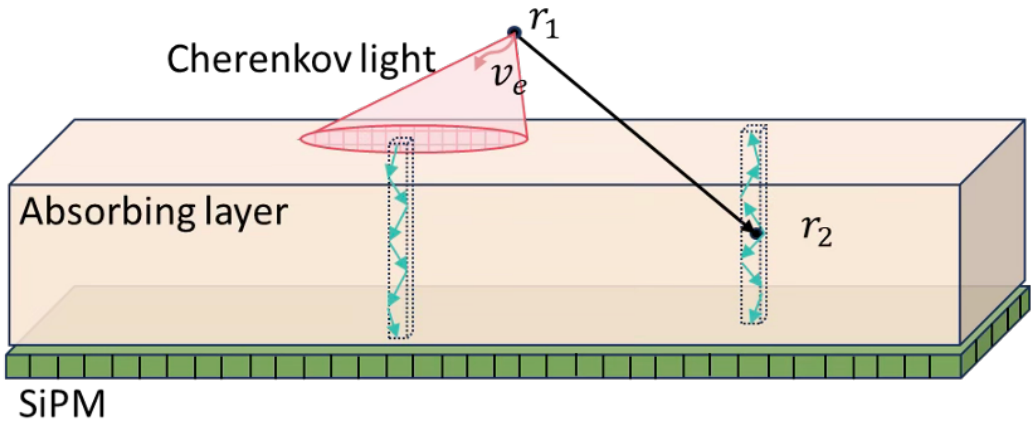

MC Sample: Dataset A1 for Training

- Simulated 500k events, ~10k effective events
- For random direction simulation, all events cover the expected incident face region, the points lie inside a circle of radius 25 mm.
- 2D endpoint density shows the number of events in each XY bin => the accepted direction density is uniform.
- Similar **Dataset A2 with various random seed**.

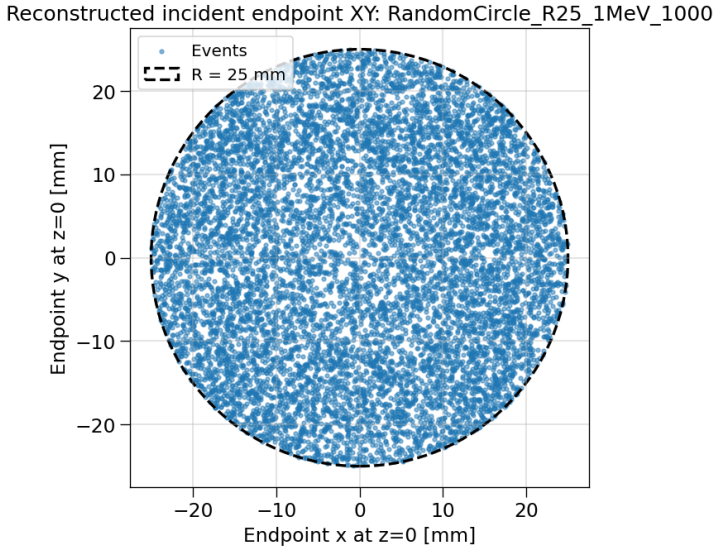

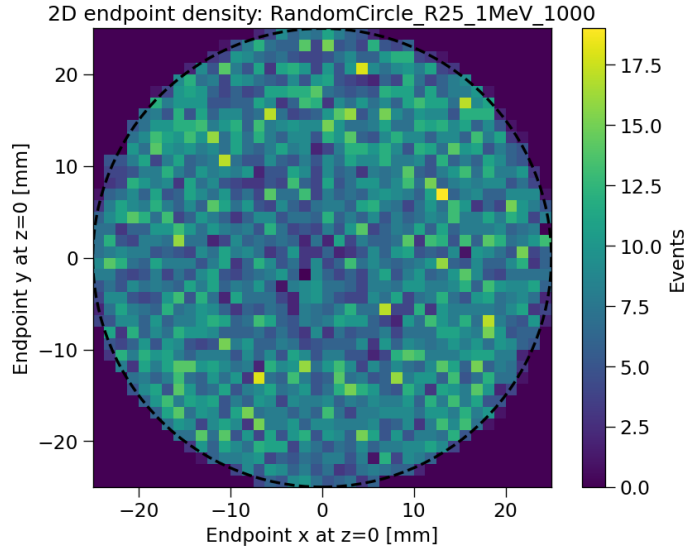

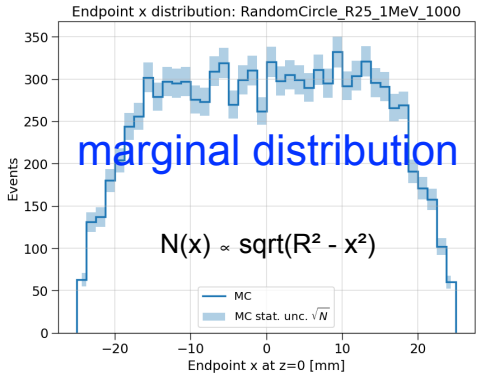

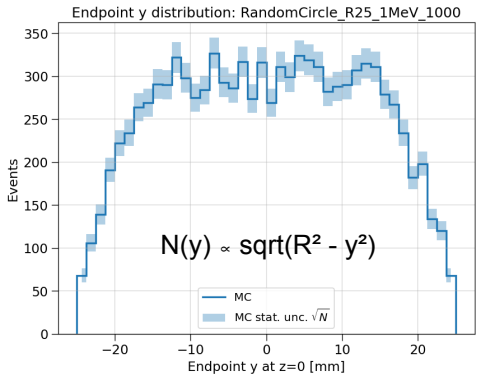

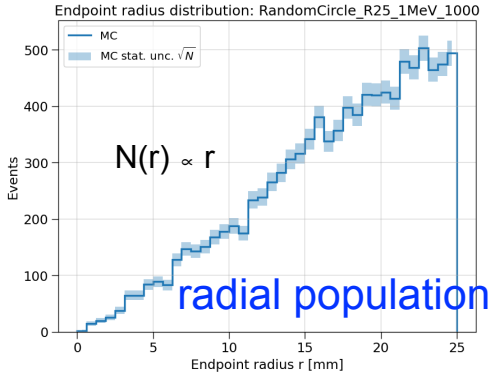

Conclusion: Uniform sampling for incident direction.

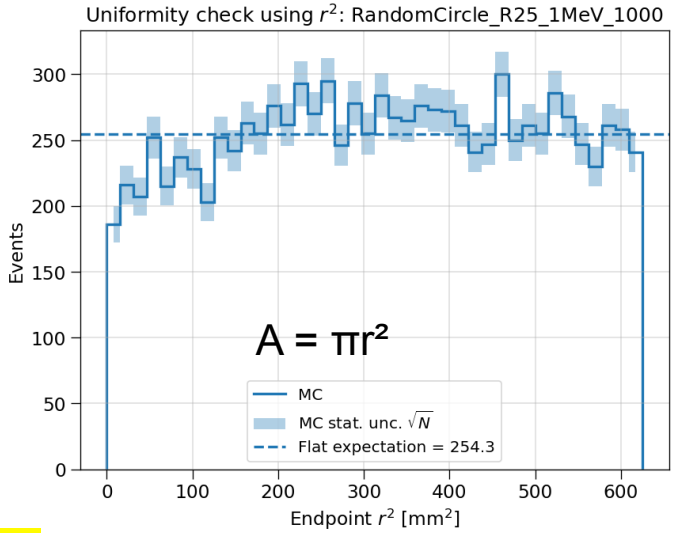

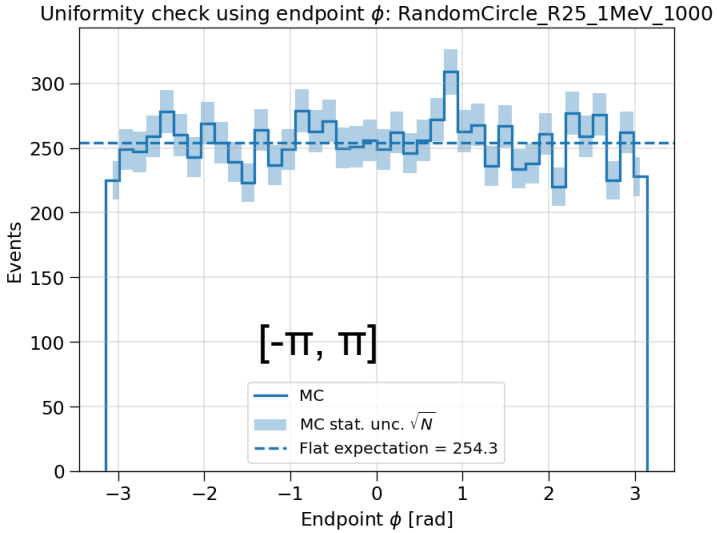

Endpoint r2 = endpoint_x_mm² + endpoint_y_mm²
Endpoint phi = atan2(endpoint_y_mm, endpoint_x_mm)

MC Sample: Dataset A2 for Inference

- Simulation setup similar to DatasetA1, but various random seed was applied.
- Simulated 500k events, ~10k effective events

marginal distribution

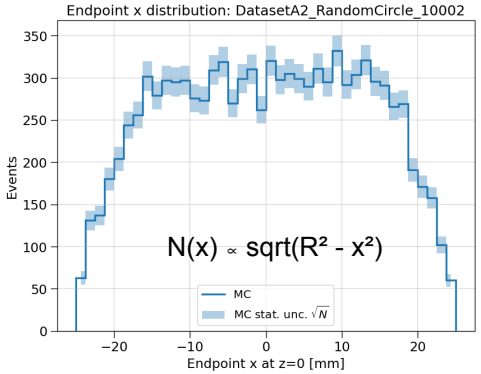

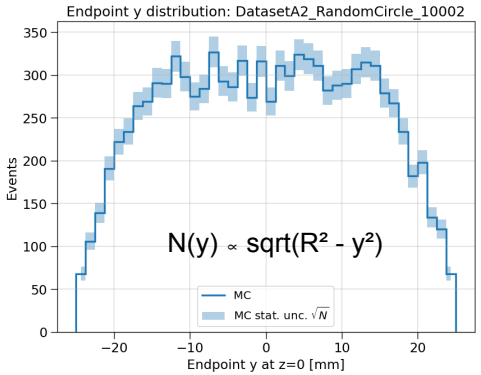

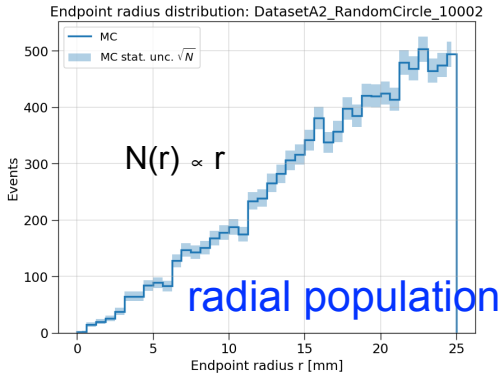

radial population

Conclusion: Uniform sampling for incident direction.

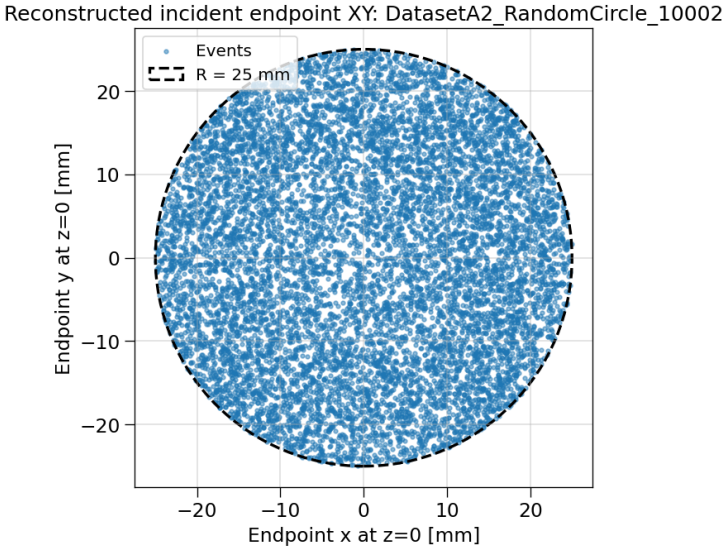

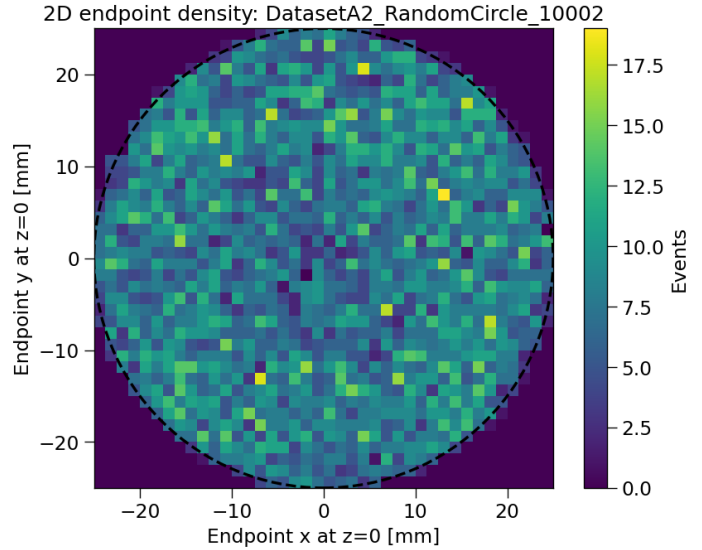

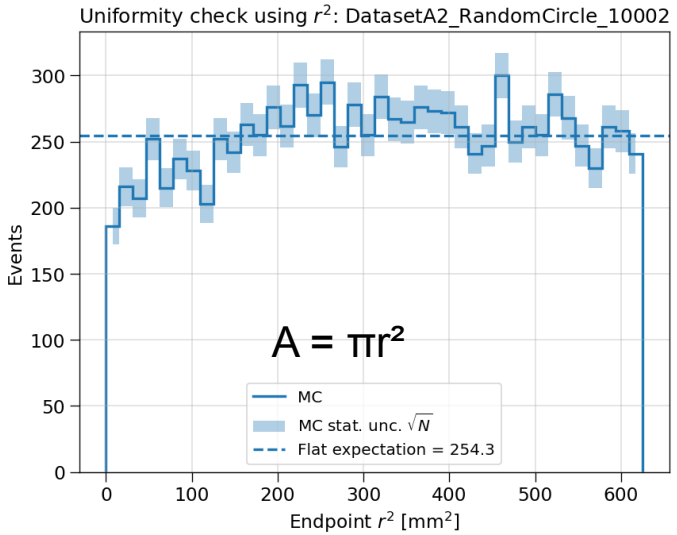

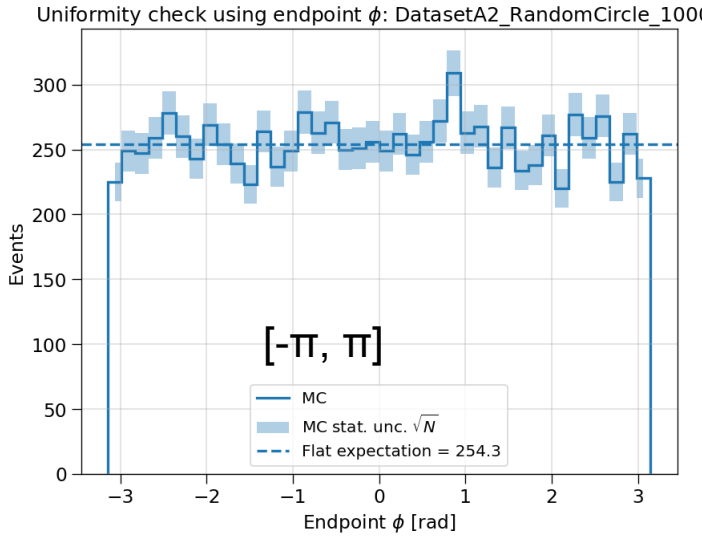

Endpoint r2 = endpoint_x_mm² + endpoint_y_mm²
Endpoint phi = atan2(endpoint_y_mm, endpoint_x_mm)

MC Samples: Dataset B for Inference

- Dataset B: fixed-grid validation sample => fixed regular grid
  - => monitor training and make resolution maps (total effective statistics: 198k events)

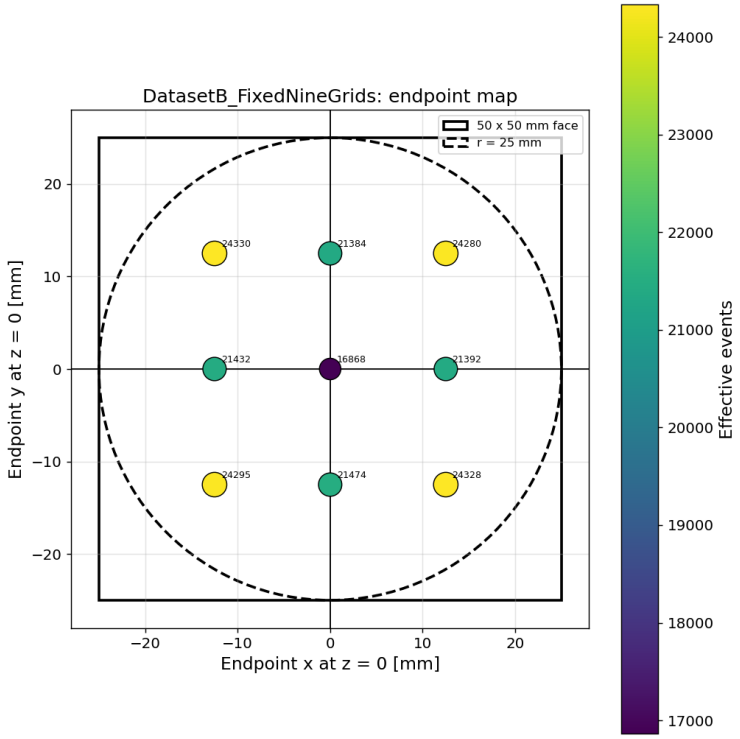

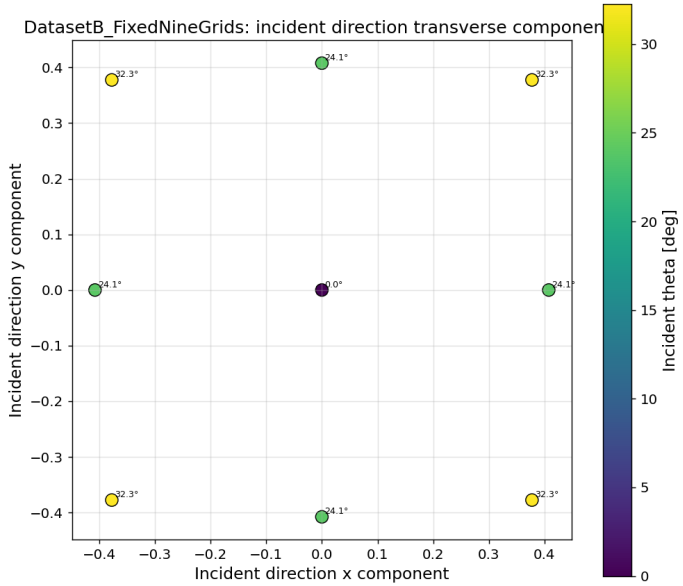

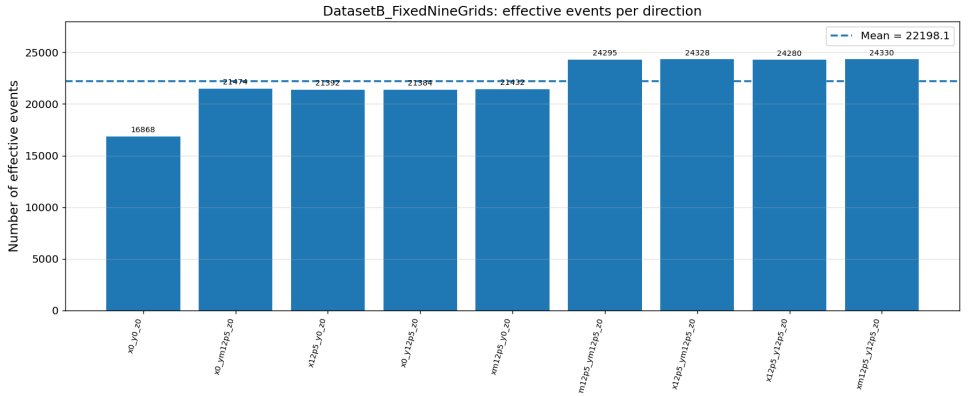

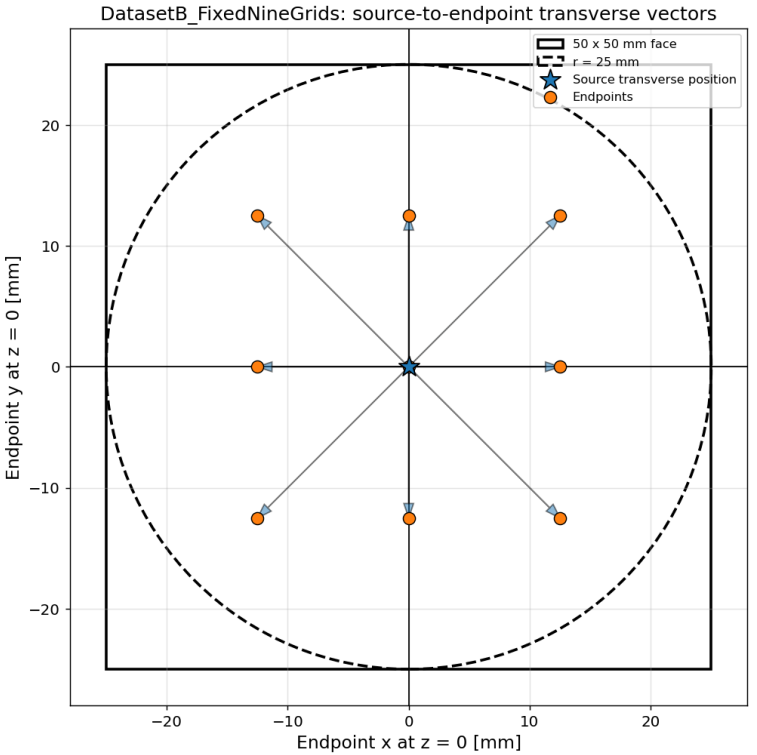

MC Samples: Dataset C for Inference

- Dataset C: shifted-grid test sample => shifted fixed grid on Dataset B
  - => test interpolation/generalization (total effective statistics: 3.2k events)

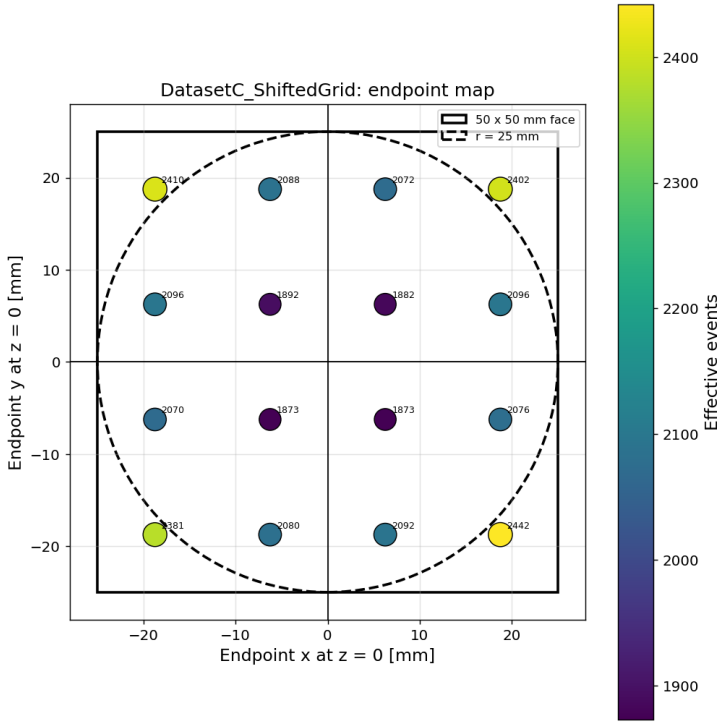

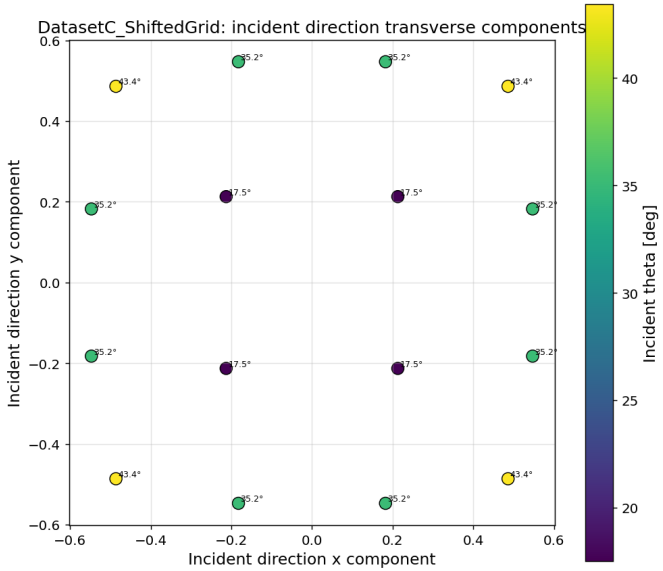

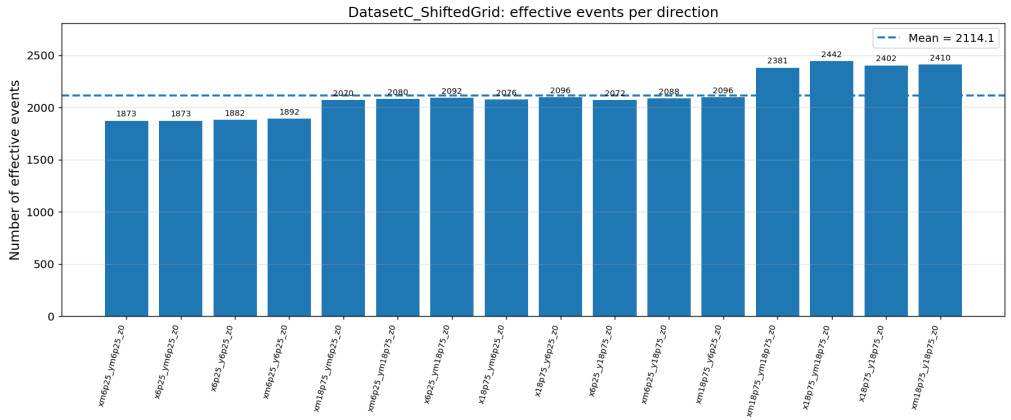

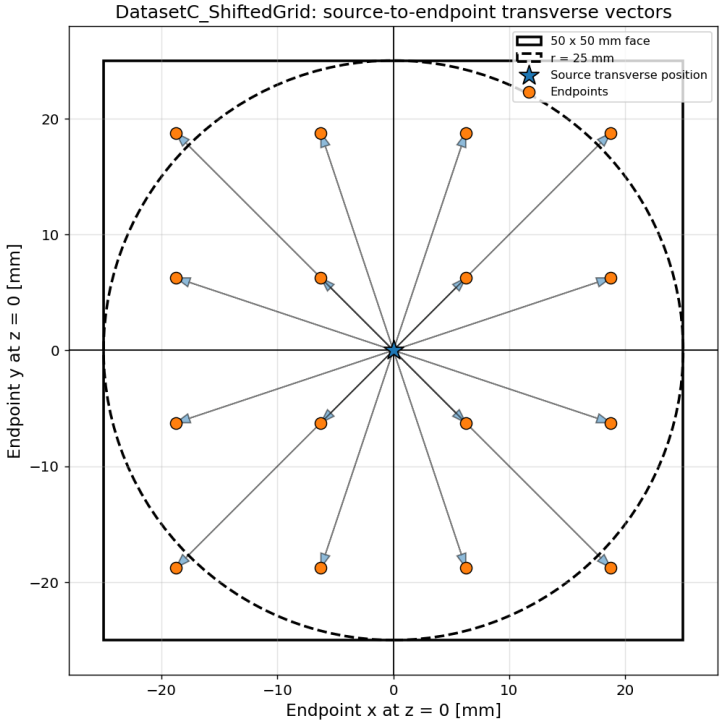

MC Samples: Dataset D for Inference

- Dataset D: radial-ring stress-test sample => fixed-radius rings
  - => test performance at large-radius boundary (total effective statistics: 64k events)

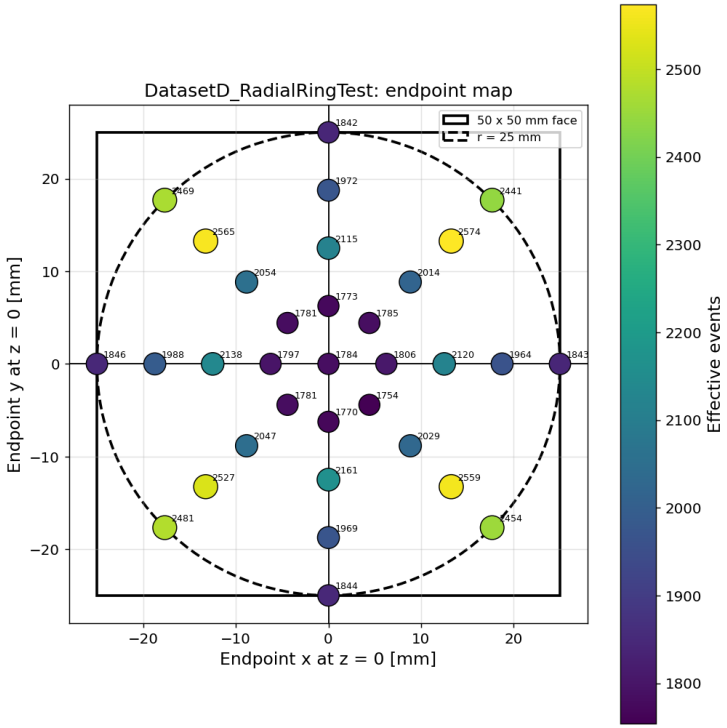

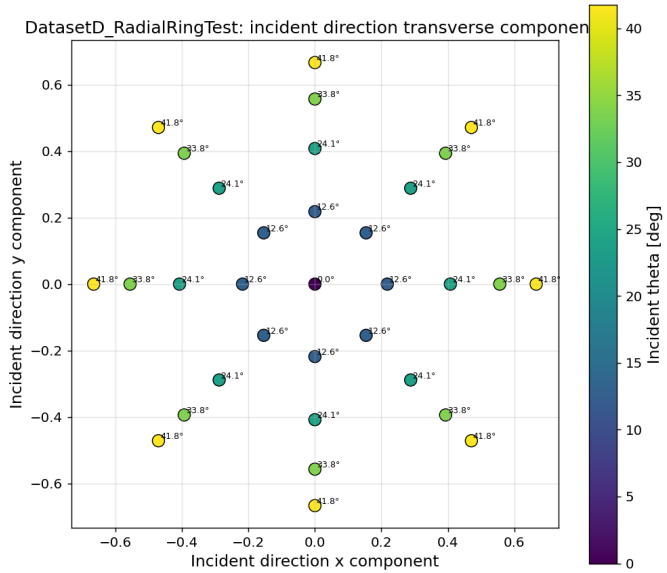

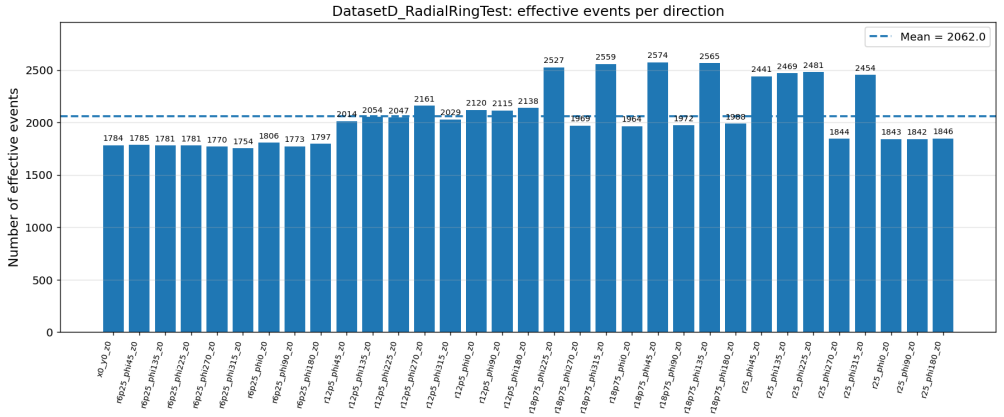

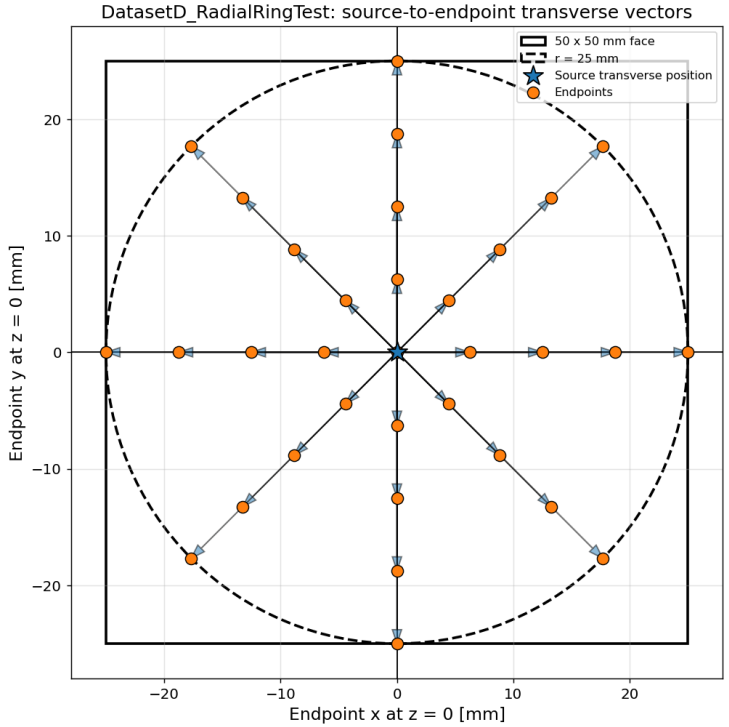

Common Reconstruction Algorithm: Likelihood

- **Reconstruction procedures**:
  - Select the "good" topology: first interaction in CsI(Tl) = Compton, second one in BGO = photoelectric
    - Calibrate E_1 and E_2 from optical photon yields
  - Reconstruct the first interaction point P_1 in CsI(Tl) with maximum likelihood
    - Get recoil-electron direction from early Cherenkov photons
  - Identify the brightest BGO spot to estimate P_2 and get scattered-photon direction from $P_1 \rightarrow P_2$
  - Combine Compton kinematics + electron direction to infer the incident gamma direction.
- **Dominant bottlenecks**:
  - P_2 mis-identification strongly biases **BGO energy** and **scattered-photon direction**.
  - P_1 has a noticeable depth bias, especially in z direction.
  - Electron-direction reconstruction is still much weaker than photon-direction reconstruction.

- The final incident-gamma direction error is therefore driven by a cascade:
  - **Position error → recoil electron / scattering photon opening-angle error → gamma-direction error**. (Used the transformer algorithm to reconstruct the directions.)

Uncertainty Sources

误差分析：

位置误差：

第一作用点：

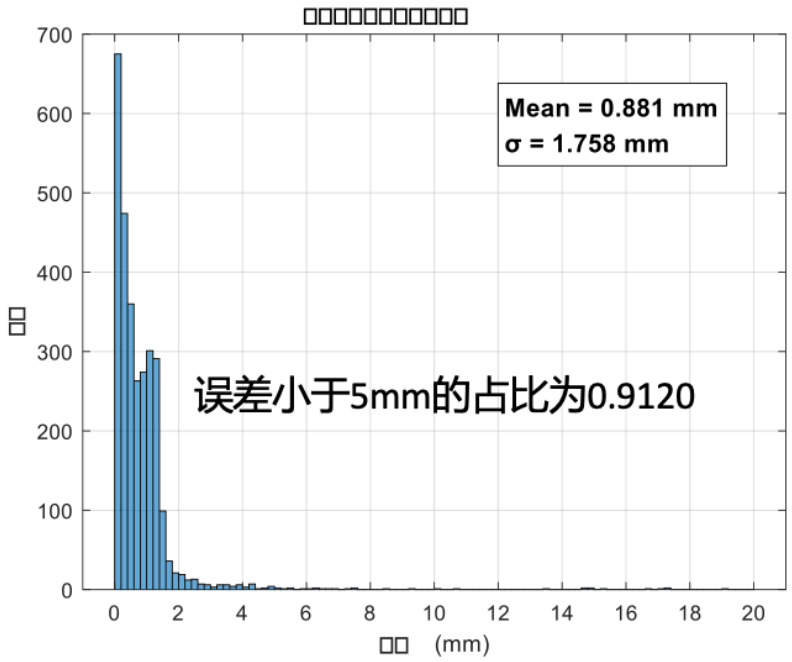

第二作用点：

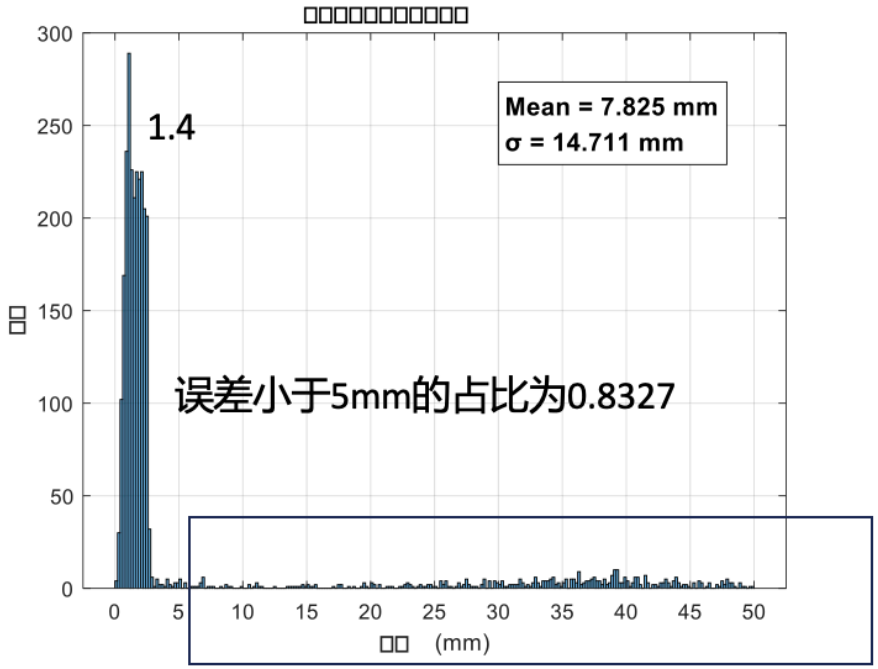

判断错误，对应能量也错误

(1) BGO能量沉积较小<300

(2) 发生作用点及其靠近某一面

Comparison with Coded Collimation

Feature	Coded collimation	Hybrid Compton camera
Imaging principle	Shadow pattern through coded mask	Reconstruct Compton event topology
Main information used	Detector-plane intensity pattern	Optical photon topology, timing, energy, positions
Event-by-event direction	Usually no; image needs accumulated counts	Yes, incident direction predicted per event
Efficiency	Limited by mask open fraction and absorption	Potentially higher, no heavy mechanical mask
Field of view	Can be moderate to wide, mask-dependent	Naturally wide field of view
Best energy range	Often good for hard X-rays / low-energy gamma rays	Designed for MeV gamma rays
Angular resolution	Set by mask pixel size, mask-detector distance, detector pitch, source statistics (latest one ~1°)	Measured by opening-angle error, currently p68 ≈ 1.6°–1.9°
Background handling	Image reconstruction/deconvolution needed	Event topology and ML-based quality selection possible
Hardware complexity	Mask + position-sensitive detector	Optical detector + SiPM arrays + reconstruction model
Main limitation	Mask blocks many photons; deconvolution artifacts	Requires accurate simulation, calibration, and ML validation

Reference: New 3D coded aperture collimator for X/gamma-ray wide-field imaging (https://cea.hal.science/cea-04792126v1/document)

Current Limitations and Further Studies

- Current preliminary results are based on idealized Geant4 simulation and selected 1 MeV events, focusing on the incident gamma direction reconstruction.
  - Need to extend to a broader MeV energy range, especially 0.3–3 MeV and 1–10 MeV.
  - Optimize the detector geometry structure.
- Detector-level calibration has not yet been fully included.
  - CsI/BGO energy calibration, SiPM gain/PDE, timing jitter, dark noise, saturation, and channel non-uniformity need to be modeled.
  - Incident energy resolution should be evaluated using $E_{\gamma}^{\mathrm{reco}} = E_{\mathrm{CsI}}^{\mathrm{reco}} + E_{\mathrm{BGO}}^{\mathrm{reco}}$.
- Effective area and detection efficiency are not yet quantified.
  - Current samples use selected events with first interaction in CsI and full energy deposition in BGO.
  - A full efficiency study should include all generated events and realistic reconstruction selections.
- Current reconstruction depends on simulation-trained deep learning.
  - Need robustness checks against geometry variations, optical-parameter uncertainties, calibration shifts, and domain gap between simulation and future data.
- Perform the simulation using a 3D object to image.

Next step: move from proof-of-principle reconstruction to mission-level performance evaluation.

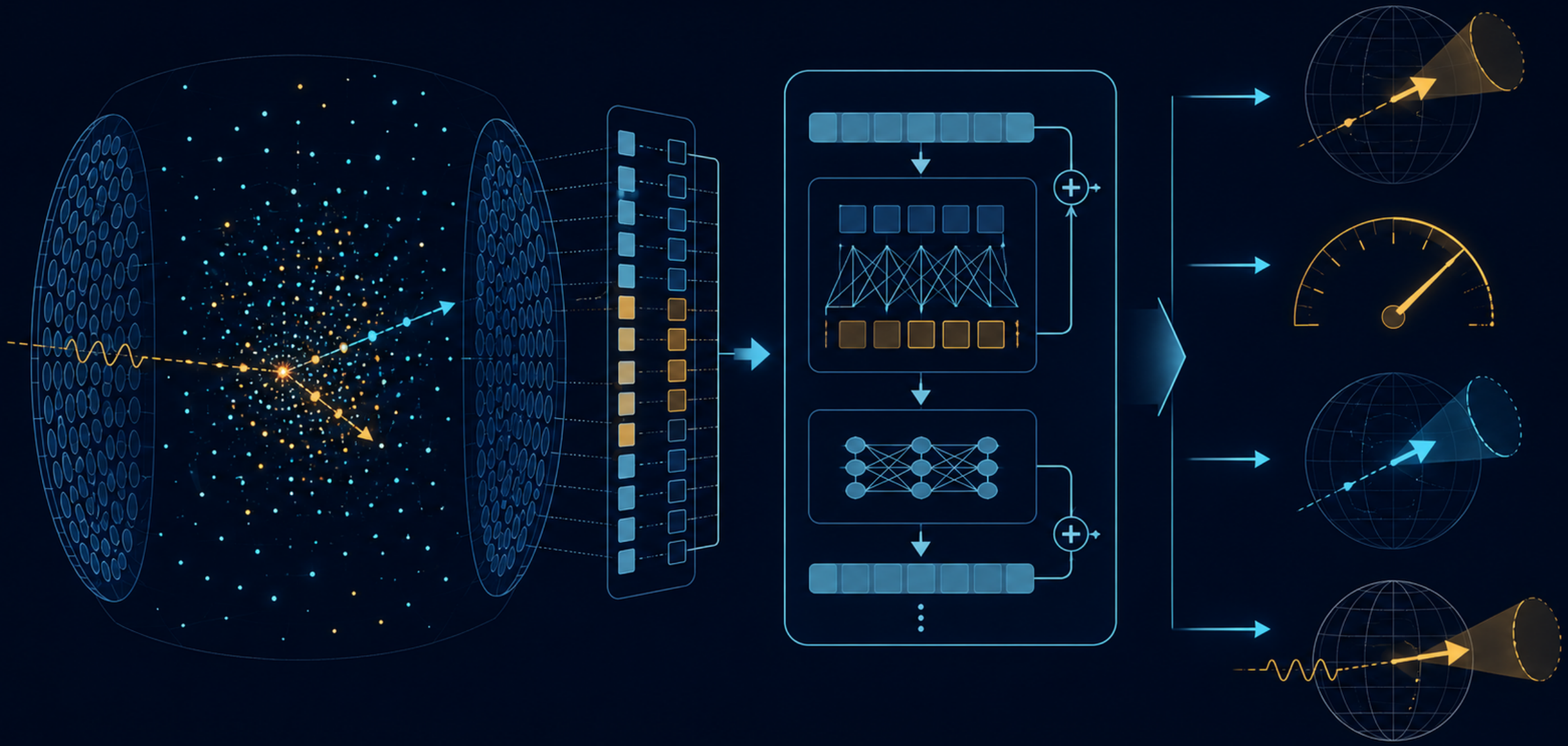

A schematic image on reconstruction logic from ChatGPT

Backgrounds

- The gamma camera is a core instrument in nuclear medicine imaging, environmental radiation monitoring, and astrophysical observation, and the present gamma cameras can be mainly classified as three categories, but all of them behave some obvious technique drawbacks in application.
  - **Mechanical Collimation Type**: Relies on mechanical collimators—typically composed of heavy metals such as lead—to restrict the direction of incoming photons. Its primary drawback is extremely low detection efficiency; furthermore, spatial resolution and sensitivity exhibit a mutually constraining relationship, making it impossible to optimize both simultaneously.
  - **Traditional Compton Scattering Type (Without Electron Direction)**: Determines the scattering angle by measuring the energy and position of photons after scattering, utilizing the Compton formula. Its disadvantage lies in the inherent ambiguity of single-event measurements (which can only define a conical surface); consequently, determining the direction of the radiation source requires the statistical superposition of a large number of photon events. This results in prolonged imaging times, rendering the method unsuitable for scenarios involving low radiation doses or rapidly changing conditions.
  - **Electron Track-Tracing Type (With Electron Direction)**: Directly records the trajectories of recoil electrons using silicon pixel detectors or Time Projection Chambers (TPCs). Its drawbacks include high system complexity and prohibitive cost. Silicon detectors require multi-layer stacking and extremely sophisticated readout electronics, and their limited thickness often prevents the complete absorption of energy; conversely, gas-based TPCs are bulky, making system miniaturization difficult to achieve. Moreover, the overlapping of electron tracks complicates the algorithmic identification of track start and end points, thereby severely compromising reconstruction accuracy.
- Consequently, achieving high-precision, single-event-level measurement of electron direction—without increasing system hardware complexity (e.g., by introducing intricate track detectors)—remains a critical technical challenge urgently awaiting resolution within this field.

Key Innovations

- Addressing the limitations inherent in the prior art, the objective of the present detector is to provide a method for locating radiation sources—as well as a corresponding gamma-ray camera device—based on the coupled detection of optical signals generated via multiple physical mechanisms. The detector leverages two distinct types of optical signals generated within a medium—Cerenkov light and scintillation light—which exhibit differing spatio-temporal characteristics, to jointly determine the state of electrons. By combining the mechanisms of Cerenkov radiation and scintillation fluorescence, the detector enables the joint reconstruction of the direction of Compton recoil electrons, thereby achieving radiation source localization at the single-event level.
- The core technical concept underlying this detector is the discovery and utilization of the distinct physical differences—manifested in both the time and spatial domains—between "Cerenkov light" (characterized by picosecond-scale transients and strong directionality) and "scintillation light" (characterized by nanosecond-scale transients and isotropy) generated by recoil electrons within a high-refractive-index medium. These physical differences are transformed into independent technical variables utilized for the reconstruction of the electron direction vector.
- The present detector encompasses the following key innovative features:
  - Dual-Modality Optical Signal Coupling Mechanism: By selecting materials with both high refractive indices and high transparency for the scattering layer, the detector compels Compton recoil electrons to simultaneously excite both Cerenkov light (utilized for direction determination) and scintillation light (utilized for energy and position determination). Through time-window separation techniques (distinguishing between picosecond-scale and nanosecond-scale signals), a single detector is enabled to simultaneously capture information derived from both modalities.
  - Composite Layered Optical Conduction Architecture:** A unique stacked structure comprising a "scattering layer—absorption layer—photodetector array" has been designed. The absorption layer functions not only as an energy absorber for secondary photons but also acts as an "optical waveguide" for the optical signals generated within the scattering layer; this design allows the underlying SiPM array to simultaneously read out reaction information from both layers, thereby significantly simplifying both the readout circuitry and the mechanical structure.
  - Single-Event Full Momentum Reconstruction Algorithm:** By integrating the principles of energy conservation and momentum conservation—and utilizing the fitting of the Cerenkov light ring to determine the initial direction of the electron—the detector completely eliminates the "cone ambiguity" inherent in traditional Compton cameras, thereby achieving the unambiguous determination of direction for individual photon events.
- This detector enables the determination of electron direction without the need for complex track-tracing hardware, thereby significantly reducing both cost and size; furthermore, it achieves single-event-level imaging, substantially enhancing detection sensitivity under low-statistics conditions.